

WIYN Open Cluster Study XI: WIYN¹ 3.5m Deep Photometry of M35 (NGC 2168)

Ted von Hippel

Department of Astronomy, University of Texas, C-1400, Austin, TX 78712
email: ted@astro.as.utexas.edu

Aaron Steinhauer

Department of Astronomy, Indiana University, 319 Swain West, 727 East Third Street,
Bloomington, IN 47405
email: aaron@astro.indiana.edu

Ata Sarajedini

Department of Astronomy, 211 Bryant Space Science Center, P.O. Box 112055, University
of Florida, Gainesville, FL 32611
email: ata@astro.ufl.edu

Constantine P. Deliyannis

Department of Astronomy, Indiana University, 319 Swain West, 727 East Third Street,
Bloomington, IN 47405
email: con@astro.indiana.edu

ABSTRACT

We present deep *BVI* observations of the core of M35 and a nearby comparison field obtained at the WIYN 3.5m telescope under excellent seeing conditions. These observations probe to $V > 26$, and display the lower main sequence in *BV* and *VI* CMDs down to $V = 23.3$ and 24.6 , respectively. At these faint magnitudes the background Galactic field stars are far more numerous than the cluster stars, yet by using a smoothing technique and CMD density distribution subtraction we are able to recover the cluster fiducial main sequence and luminosity function to $V = 24.6$. We find the location of the M35 main sequence in these CMDs to be consistent with earlier work on other open clusters, specifically NGC 188, NGC 2420, and NGC 2477. We compare these open cluster fiducial sequences to stellar models by Baraffe et al. (1998),

¹The WIYN Observatory is a joint facility of the University of Wisconsin-Madison, Indiana University, Yale University, and the National Optical Astronomy Observatories.

Siess et al. (2000), Girardi et al. (2000), and Yi et al. (2001) and find that the models are too blue in both $B - V$ and $V - I$ for stars less massive than $\sim 0.4 M_{\odot}$. At least part of the problem appears to be underestimated opacity in the bluer bandpasses, with the amount of missing opacity increasing toward the blue. M35 contains stars to the limit of the extracted main sequence, at $M \approx 0.10\text{--}0.15 M_{\odot}$, suggesting that M35 may harbor a large number of brown dwarfs, which should be easy targets for sensitive near-IR instrumentation on 8–10m telescopes. We also identify a new candidate white dwarf in M35 at $V = 21.36 \pm 0.01$. Depending on which WD models are used in interpreting this cluster candidate, it is either a very high mass WD ($1.05 \pm 0.05 M_{\odot}$) somewhat older (0.19–0.26 Gyr, $3\text{--}4\sigma$) than our best isochrone age (150 Myr), or it is a modestly massive WD (0.67–0.78 M_{\odot}) much too old (0.42–0.83 Gyr) to belong to the cluster. Follow-up spectroscopy is required to resolve this issue.

Subject headings: Galaxy: stellar content – open clusters and associations: individual (NGC 2168) – stars: luminosity function – white dwarfs

1. Introduction

NGC 2168 (M35) is a rich open cluster with an age similar to the Pleiades. Since M35 is more populous and covers a smaller angular extent than the Pleiades, it offers excellent opportunities for studies of stellar evolution at ~ 100 Myr, even though M35 is further away and suffers greater background contamination. Astrometric studies of M35 have a long history (Ebbighausen 1942; Meurers & Schwarz 1960; Lavdovskij 1961; Cudworth 1971; McNamara & Sekiguchi 1986a), and in fact continue to this day—M35 is *the* astrometric calibrator for the HST Fine Guidance Sensors (McArthur et al. 1997). Modern photometric studies of this cluster begin with Sung & Lee (1992) who obtained photoelectric UBV photometry for 112 field plus cluster stars to $V = 14$, approximately the same limiting magnitude as the two more recent proper motion studies. Sung & Lee derived a true distance modulus of 9.3, an age of 85 Myr, and internal differential reddening of $0.26 \leq E(B - V) \leq 0.44$. In a subsequent study, Sung & Bessel (1999) obtained $UBVI$ CCD photometry for stars brighter than $V = 20$ in a central $20'.5 \times 20'.5$ cluster field. From these data they derived $(V - M_V)_0 = 9.6 \pm 0.1$, $E(B - V) = 0.255 \pm 0.024$ (corresponding to $(V - M_V) = 10.39$ for $R_V = 3.1$), $\log \text{age} = 8.3 \pm 0.3$ (200 Myr), $[\text{Fe}/\text{H}] \approx -0.3$

(based on $U - B$ color excess), a present day mass function slope of -2.1 ± 0.3 ,² and a binary frequency $\geq 35\%$. A younger cluster age of 70 to 100 Myr was found by Reimers & Koester (1988a), based on a reanalysis of older photometry along with isochrones from Maeder & Mermilliod (1981) and on the cooling age of two cluster white dwarfs. Barrado y Navascués, Deliyannis, & Stauffer (2001a) have derived the cluster metallicity, $[\text{Fe}/\text{H}] = -0.21 \pm 0.10$, from high resolution spectroscopy. In the most recent photometric study of M35, Barrado y Navascués et al. (2001b, hereafter BSBM), using the Kitt Peak 4m and CFH 3.6m telescopes, imaged the central $28' \times 28'$ of the cluster in VRI to $V \approx 22$ and $I \approx 23$. BSBM found a luminosity function similar to the Pleiades, with a peak near $M_I = 9$, and present-day mass function characterized by three different power law slopes over the mass range 1.6 to $\sim 0.1 M_\odot$. BSBM found their central cluster field to contain $\sim 1600 M_\odot$ among cluster members.

In a dynamical study of M35, Leonard & Merritt (1989) found that M35 is close to dynamical equilibrium, that its dynamical mass within the central 3.75 pc is 1600 to 3200 M_\odot (95% confidence), and that its IMF slope is -2.7 ± 0.4 between 1 and 6 M_\odot . Mathieu (1983), McNamara & Sekiguchi (1986b), and BSBM all noted that M35 exhibits mass segregation, though it is unclear whether this is due to relaxation or initial conditions. Mathieu (1983) pointed out that the cluster age is close to the expected relaxation time of the intermediate mass component, though the relaxation time scale is uncertain by a factor of 2.

We obtained deep BVI photometry of M35 in order to study the low mass main sequence stars and to search for cluster white dwarfs. Our study presents higher signal-to-noise data for the faintest stars than the BSBM study, and we achieve this depth in B , V , and I , whereas BSBM achieve their greatest depth in R and I . Our photometry allows us to isolate the fiducial main sequence of the cluster in B and V , as well as V and I , which we compare to a range of stellar models. The smaller field of view of our study precludes a detailed luminosity function or mass function study, however, as done by BSBM. In these trade-offs between field of view and depth in various filters, our two deep photometric studies are complementary. In addition, we have found a candidate cluster white dwarf which, if a *bona fide* cluster member, places constraints on a combination of cluster age and stellar evolution.

²All mass function slopes presented here are on the system $n(m) \propto m^{-(1+x)}$, where the reported slope = $-(1+x)$, and the Salpeter (1955) value is -2.35 .

2. Data Reduction

We observed M35 and a nearby comparison field at the WIYN 3.5m telescope located on Kitt Peak through Harris B - and V -band and Mould interference I -band filters (Massey et al. 1987) on the nights of December 31, 1997, January 1, 1998, and January 22, 1998. All of these nights were non-photometric, though the seeing was excellent, ranging from 0.46 to 1.0 arcseconds FWHM, with the majority of the observations obtained during 0.6 to 0.8 arcsecond seeing conditions, even in the B -band. Total exposure times of 4500, 3357, and 7200 seconds in B , V , and I , respectively, were obtained on a field centered on M35, at $RA = 06^h08^m54^s$, $Dec = +24^\circ17'53''$ (2000), corresponding to Galactic coordinates l , $b = 186.62$, 2.17 degrees. Total exposure times of 4500, 4500, and 9000 seconds in B , V , and I , respectively, were obtained in a nearby comparison field, located at $RA = 06^h08^m54^s$, $Dec = +24^\circ33'59''$ (2000), corresponding to l , $b = 186.39$, 2.30 degrees.

The CCD detector then in use at WIYN, “S2KB,” is a 2048^2 STIS CCD with 21 micron ($=0.2''$) pixels and a field of view of 6.8×6.8 arc minutes. Data reduction followed standard procedures virtually identical to those described for the old open cluster NGC 188 by von Hippel & Sarajedini (1998, hereafter WOCS1). Briefly, we removed a time-dependent, two-dimensional bias structure with the help of the overscan regions and standard bias frames to within a typical accuracy of 1 ADU. For these broad-band exposures the high sky meant that this bias uncertainty was always much less than 1%. Flat fielding was performed using dome flats with typical pixel-to-pixel Poisson uncertainties of $\leq 0.25\%$ and illumination pattern uncertainties $\lesssim 1.0\%$.

Instrumental magnitudes were extracted from each image individually using ALLFRAME (Stetson 1994). We employed a quadratically varying PSF, defined using the brightest 50–100 isolated stars, and refined by iteratively subtracting faint neighbors. These PSFs along with a master coordinate list of stellar positions for each field were input into ALLFRAME which then produced total PSF magnitudes for all detected profiles. The PSF magnitudes measured for each frame were corrected to total magnitudes by applying a spatially variable aperture correction. The amplitude of this correction was never more than ± 0.02 mag but was nevertheless applied to maximize the accuracy of the resultant photometry. We edited the photometry using fitting quality diagnostics provided by ALLFRAME. In particular, we set a maximum overall CHI value of 2.5 and a maximum mean magnitude error in 0.5 mag bins of 2σ . We also stipulated that the distribution of SHARP values be symmetric around zero and thus edited outlying SHARP values until this was accomplished.

Since the nights were not photometric, the WIYN data were placed on the standard system of Landolt (1983, 1992) using photometric, calibrated BVI observations (Deliyannis

et al. 2002) of the central $23' \times 23'$ of M35 taken on the night of October 24, 1998 with the KPNO 0.9m telescope. The 0.9m M35 observations were first calibrated via the Landolt standards, and then the 0.9m data were used to calibrate the WIYN data. The details of the standards observed to calibrate the 0.9m M35 observations are presented in Table 1. Column 1 lists the filter in question, with two different color calibrations given for the V -band, one based on the $B - V$ color and the other based on the $V - I$ color. Column 2 lists the number of independent CCD frames taken of the standard fields, column 3 lists the number of standards used to derive the photometric transformations, columns 4 and 5 list the photometric zero points and their associated errors, columns 6 and 7 list the derived airmass coefficients and their errors, and columns 8 and 9 list the derived color terms and their errors. The standard observations spanned the same UT range as the cluster observations, though not the same airmass range. The airmass range for the standards was 1.18–1.64, whereas the cluster was observed over a lower and more restricted airmass range, 1.01–1.06. While the Landolt standards were observed at a slightly higher minimum airmass than M35, this was unavoidable given our desire to observe M35 at the lowest possible airmass, whereas the Landolt fields are located on the celestial equator. The airmass terms were linear, so this extrapolation to airmass = 1.0 (from airmass = 1.18) should have a minimal effect on the standardization. In our standardization procedure we define the color terms for all filters with respect to V . For the V calibration, $B - V$ was used preferentially. However, the $V - I$ color term was also calculated for V , and used when a B magnitude was not available for a given program star. This allowed us to take full advantage of our greater photometric depth in V and I than in B . The color terms were linear, small, and had tiny uncertainties.

While the 0.9m M35 observations probed to $BVI = 20$ – 21 , ~ 5 mag shallower than the WIYN observations, there remained > 4 magnitudes of overlap between the two data sets, and the stars in common cover much of the range in color (for B the range was $B - V = 0.92$ – 1.89 and for VI the range was $V - I = 0.17$ – 2.28). We thus calibrated the WIYN photometry from the many (92 to 292, depending on the filter and field) stars in common with the 0.9m photometry. We calculated transformations between the two data sets, taking into account possible changes in the color dependence of the offset. For the B filter, the following equations were solved:

$$(B - V) = a_1 (b - v) + c_1 \quad (1)$$

$$b - B = a_2 (B - V) + c_2 \quad (2)$$

where b and v are instrumental magnitudes and B and V are standard magnitudes. The constants were empirically determined. Similar equations were used to standardize the

V and I data using the $V - I$ color in the transformation.

Based on experience with these instruments and similar data, we estimate the total systematic error of our standardized photometry to be $\lesssim 0.02$ mag. Note, however, that the reddest Landolt standard we used had $B - V = 1.9$ and $V - I = 2.4$, whereas our data continue to $B - V = 2.4$ and $V - I = 4.0$. Since the color terms for the lower main sequence are extrapolations, the photometry for the reddest stars is likely to be less accurate than the numbers quoted above. Since the reddest stars are of particular importance in this study we explored two avenues to constrain any possible systematic shifts in the photometry. In the first approach, we perturbed all the photometric transformation coefficients by $+1\sigma$ and by -1σ . This approach only indicates whether errors in the transformation coefficients themselves matter in the extrapolation, of course, and not whether different transformation coefficients are appropriate for the reddest stars. The mutual probability that all four (per filter) transformation coefficients would be each wrong by $+1\sigma$ or -1σ is $< 5\%$ (i.e., a 2σ error). This 2σ envelope at the very bottom of the main sequence corresponds to only $\Delta(B - V) = \pm 0.09$ and $\Delta(V - I) = \pm 0.014$. This small error range is gratifying and due to the fact that the color terms are small and linear, and the photometric calibration, especially in V and I , was excellent. As a second constraint on any systematic errors in the color terms we performed synthetic photometry for a range of F0V to M6V stars from the Pickles (1998) spectral library, using the tracings for the WIYN filters and the measured quantum efficiency versus wavelength for the S2KB CCD. The synthetic photometry was compared to standard $B - V$ and $V - I$ colors for stars of the same MK type compiled by Johnson (1966). Overall we found excellent agreement between our synthetic color terms and those we derive from the standard star observations, except for the very reddest stars where our synthetic photometry indicated that our extrapolated color terms may make the faintest cluster members too blue in both $B - V$ and $V - I$ by 0.1 to 0.2 mag. We do not apply the offset indicated by the synthetic photometry, but rather use it as a guideline to the level of the likely systematic color error at the limit of the main sequence. This level of error is acceptable and less than the differences we will explore between the data and stellar models.

As a final step in the data reduction process, we measure image morphology using SExtractor (Bertin & Arnouts 1996) in order to reject non-stellar objects. SExtractor has the advantage of determining sky locally and uses verified neural network techniques to perform the star/galaxy classification. Figure 1 shows the results of the SExtractor morphological classification versus I -band magnitude for both the M35 and control fields. The morphological “Stellarity Index” ranges from 0 for galaxies or obvious imaging defects to 1 for stars. Although SExtractor’s neural network classifier is not strictly a Bayesian classifier, the Stellarity Index values are approximately the probabilities that the object is

a point source. The classifications near 0.5 at the faintest magnitudes demonstrates the common sense notion that at limiting signal-to-noise classification breaks down. Objects from the M35 central field are plotted as small filled circles. Objects from the control field are plotted as small open circles and shifted down by 0.1 and to the right by 1 mag, so that both data sets can be clearly seen in the same plot. Figure 1 demonstrates that the morphological-magnitude distribution of objects in both fields is essentially identical, the result of observations obtained under excellent and stable conditions. The large number of definite stars in Figure 1 is the result of a cluster plus a rich Galactic field, and the significant suppression of background galaxies is caused by the high line-of-sight absorption in front of and behind M35. Still, there is extragalactic contamination, which we now remove.

We select those objects determined by SExtractor to have a high (≥ 0.95 , marked by the dashed lines in Figure 1) probability of being stars based on their I -band morphology, since the I -band is the deepest and best resolved, particularly for the faintest red cluster stars. While some of the objects with lower stellarity indices may be stars, we wish to be conservative in our attribution of objects to the cluster, especially at the faintest magnitudes and intermediate colors, where galaxies may contribute significantly to the number counts. As it turns out, there are few contaminating galaxies brighter than $I = 22$, above which we have excellent morphological classifications. For $I \leq 22$, we reject only 3.5% and 1.2% of the objects in the central and control field as being non-stellar, respectively. Fainter than this limit the morphological classifications begin to degrade, but this is so faint, particularly on the main sequence where it is equivalent to $V = 26$, that it has no effect on any of the statistical cluster quantities that we derive.

The cleaned and calibrated color magnitude diagrams (CMDs) are presented in Figures 2a through 2d. In these figures the morphological criterion is essentially equivalent to a signal-to-noise cut (at ~ 15) in the I -band. Since the B - and V -band observations are shallower than the I -band observations, however, the limiting depths in Figures 2a-d are not due to our morphology statistic. Individual error bars are not plotted for clarity but typical photometric errors at each integer V -band magnitude starting at $V = 16$ are presented down the right-hand sides of Figures 2a-d. These errors are internal errors only.

3. Discussion

The dynamic range of our WIYN observations is approximately 10 magnitudes, with the cluster main sequence evident over 8 or 9 magnitudes. For comparison, note that the cluster turn-off is another 7 magnitudes brighter than the brightest photometry presented

here, at $V \approx 8$. Although M35 is a rich cluster, as is particularly evident along the well-populated upper main sequence (see figure 3 of Sung & Bessell 1999) or from wide field images such as the Palomar Observatory Sky Survey, when viewed in deep CMDs as presented here, there are clearly far fewer stars belonging to M35 than to the background Galactic field. This is expected given the low Galactic latitude and the tremendous volume surveyed behind the cluster. Typical field stars are 1 to 4 mags fainter than the cluster main sequence at a given $B - V$ or $V - I$ color. Even though most of these objects are main sequence stars, they still reside at distances of 1.6 to 6.3 times further away than the cluster, and thus these CMDs survey a huge volume of the background Galactic disk.

Even with the copious background, the cluster main sequence is discernible in the central field, and possibly in the control field. At $16'.1$ north of the cluster center, our control field may not completely avoid cluster stars. This will be discussed in a statistical context, below. (In fact, the control field was initially selected to be within the cluster periphery so that we could measure luminosity functions in both the cluster center and periphery in order to look for signatures of mass segregation. The low number density of faint cluster stars precluded that comparison, but left us with a very useful control field that is a good compromise between avoiding the cluster entirely and moving so far away that the background field is not comparable—a potential problem given the steep gradient in stellar counts near the Galactic plane and the variable, though not large, reddening in this field.) Visually, the cluster main sequence can be traced to $V \geq 25$ in the $V - I$ CMD. The cluster binary sequence is not obvious in these CMDs (more on this later). Finally, a few blue objects between $V = 21$ and $V = 22$ can be seen in both the central and control field CMDs. We explore the likelihood that any of these objects are cluster white dwarfs and the implications for the cluster and white dwarf physics below.

3.1. Cluster Parameters

We adopt the cluster parameters from our wide-field study in preparation (Deliyannis et al. 2002), i.e., $(m - M)_V = 10.15$, $E(B - V) = 0.20$, and age = 150 Myr, although we will check the validity of the distance and reddening assumption based on fitting the 0.9m main sequence photometry to other cluster main sequences observed by Hipparcos (Pinsonneault et al. 1998). We also adopt $E(V - I) = 1.34 E(B - V)$ based on the central wavelengths of the WIYN V and I filters and the relations of Cardelli, Clayton, & Mathis (1989). Note that our distance and reddening are roughly consistent with, but not identical to, those used by BSBM, who adopted $E(B - V) = 0.255$ from Sung & Bessell (1999) and who used an I -band distance modulus corresponding to $(m - M)_V = 10.37 \pm 0.1$. Before performing

the main sequence fitting, we first extract the cluster fiducial sequence by employing our control field to remove the contaminating Galactic field stars.

3.2. Removing Field Star Contamination

The M35 and comparison fields were observed to similar depths under similar conditions, presenting us with sufficient data to perform a good statistical subtraction of the contaminating field stars. As a first attempt at this subtraction we identified nearest neighbors in the central and control CMDs, then subtracted them. We also tried variants on this technique where the number of objects in boxes of different sizes were computed in each CMD, then subtracted. This entire approach proved unsatisfactory and it became clear that an appropriate form of smoothing was required. If each CMD is thought of as an estimated density distribution, then the difference between a cluster field CMD and a control field CMD becomes the difference between two estimated density distributions. As advised by Silverman (1986), we first smoothed the CMDs with an Epanechnikov kernel. The Epanechnikov kernel is an inverted parabola that places the peak density at the object position and zero density at plus and minus the kernel width. This smoothing was performed using software kindly provided by K. Gebhardt (for examples of its use in astronomy see Gebhardt et al. 1995, 1996). We tried a variety of Epanechnikov kernel sizes (smoothing lengths), ranging from 0.01 mag to 1.0 mag and found that 0.10 mag represented the best compromise between maintaining the original resolution of the CMDs and smoothing the CMDs enough so that the subtraction did not contain too much high frequency noise.

A slight complication in the CMD subtraction was that the comparison field is slightly less reddened than the cluster field. This difference was unsurprising given the known variable reddening in the vicinity of the cluster. The decreased reddening in the comparison field relative to the central field was measured by fitting the blue edge of the field stars in the CMD in three different magnitude ranges. We estimate the reddening difference to be $\Delta E(B - V) = 0.05$. Although this reddening difference is almost certainly spread out in distance along the line of sight, we approximate it as a single value for all stars in the comparison field, and apply a single offset in color and luminosity to the control field CMDs. Small errors in this reddening offset and the limitations of using a single reddening value will make our subtraction process noisier, but will not meaningfully affect the location of the derived fiducial cluster sequences. Note that alternative explanations for the color offset between the cluster and comparison fields, e.g., due to stellar population differences, are unlikely. These two fields are near enough to one other that the Galactic model of Reid

& Majewski (1993) yielded essentially identical CMDs for both fields. Additionally, the VI CMD for the comparison field had slightly more stars than its counterpart for the cluster, 1554 stars versus 1463 stars, despite the fact that the comparison field is at a slightly higher Galactic latitude, $b = 2.30$ versus $b = 2.17$. The excess is primarily at the bottom of the CMD, past $V = 25.3$, consistent with expectations of less absorption for this field.

Figure 3a presents a smoothed (kernel = 0.10 mag) VI CMD for the central cluster field and Figure 3b presents a similar VI CMD for the control field, artificially reddened by $E(B - V) = 0.05$. Figure 3c presents the subtracted CMD. For Figures 3a through 3c the horizontal axes are $V - I$ color from 0.0 to 4.5 and the vertical axes are V magnitude from 15 to 26. Figure 3c also presents the best fit fiducial sequence as a white line. The fiducial sequence has been shifted downward by 0.30 mag for presentation purposes, to make it easier to visually identify the cluster main sequence. While there is some subtraction noise elsewhere in the CMD, seen as black points which are negative star counts, the cluster main sequence is almost entirely positive. Due to the limited statistical significance of the presence of the main sequence above $V = 17.7$ in these WIYN data, the fiducial sequence above that limit was derived from the wide-field 0.9m data (Deliyannis et al. 2002), and checked for consistency in these data. We created similar smoothed and subtracted BV CMDs.

3.3. Fiducial Main Sequence and Distance

We extracted the cluster fiducial main sequence from the VI (Figure 3c) and BV subtracted density maps by identifying peaks in the main sequence region. Because of the small number of stars involved we found it easiest to first identify the main sequence by eye, then statistically validate and improve our choice of main sequence location by computing star counts in regions around the nominal fiducial sequence. Star counts determined in regions around the correct main sequence location should asymptote to a constant value after a sensible extraction width has been reached since only in the main sequence region should there be excess star counts in the difference maps. To demonstrate this point, the solid curve cutting through the circles in Figure 4 presents the cumulative number of stars extracted along the entire V -band magnitude range ($19.82 \leq V \leq 24.62$) of our initial WIYN VI fiducial sequence as a function of the width of the extraction window. The smallest extraction window considered was ± 0.00 mag, i.e., along the 0.01 width of this fiducial sequence. The largest window considered was ± 0.5 mag, for a total width of 1.01 mag. Once the window width reached 0.29 mag (± 0.14 mag around the fiducial sequence) the total number of stars in the LF remained constant, at 47. The quality of the subtraction

around the main sequence region remains good even with a window width as large as ~ 0.7 (± 0.35) mag. Besides the curve indicating cumulative star counts around the initial fiducial sequence as a function of $V - I$ window width, a series of other curves are plotted, each for a different fiducial sequence created by offsetting the initial fiducial sequence by ± 0.025 , 0.05 , 0.075 , 0.10 , and 0.125 mags. The $+0.025$ mag offset (redward) represents a slight improvement over our initial fiducial sequence, and we adopt this improvement for our best estimate of M35’s fiducial sequence. Figure 4 also serves to yield an overall $V - I$ error in the fiducial sequence: The five curves containing the most stars within the smallest color range present the reasonable range of the best fit, yielding an overall uncertainty in the fiducial sequence of $\Delta(V - I) = \pm 0.05$.

The identical procedure was used for the BV cluster fiducial, where we found a color uncertainty, $\Delta(B - V) = \pm 0.03$. While our procedure does not justify the subtle wiggles in the BV and VI fiducial sequences, it does justify the overall fiducial location, particularly for $V > 22.5$, where the bulk of the cluster stars are found, and where we will focus our comparison with stellar models in the next section.

For presentation purposes and as a consistency check on the cluster distance, we extended the WIYN fiducial sequences to brighter stars ($V \leq 16.52$, $B - V \leq 1.1$ and $V \leq 17.5$, $V - I \leq 1.5$), using the 0.9m photometry of Deliyannis et al. (2002). The bright fiducial sequences are estimated by eye without the aid of the CMD subtraction technique discussed above. We estimate the errors in the bright fiducial fits to be ± 0.10 – 0.15 mag in V for a given $B - V$ or $V - I$ color, for $V \geq 17$. In the overlap region, between $V = 17$ and 20 , where the 0.9m data are not as precise and where the WIYN data contains fewer cluster stars, the error is approximately ± 0.20 mag. The BV and VI fiducial sequences are presented in Tables 2 and 3, respectively. Note that these fiducial sequences are presented in the observed system. To convert to the absolute system, M_V and $(B - V)_o$ or $(V - I)_o$, the user can apply our preferred distance and reddening ($(m - M)_V = 10.15$, $E(B - V) = 0.20$) or their own, along with $E(V - I) = 1.34 E(B - V)$, appropriate for these filters.

The upper part of the fiducial sequence, assuming our adopted cluster parameters, is compared in Figure 5 to the Hipparcos cluster fiducial main sequence derived by Pinsonneault et al. (1998). The Hipparcos fiducial is based on five nearby open clusters (α Per, Coma Ber, Hyades, Pleiades, and Praesepe) and valid over the range $0.55 \leq (V - I)_o \leq 0.9$. Although Pinsonneault et al. find a systematic problem with the Pleiades parallaxes, they argue that the other four open clusters are consistent with the same fiducial sequence within very stringent limits. They conclude that with good data one can derive the distance to a near solar metallicity open cluster using the main-sequence fitting technique to an accuracy in the distance modulus of 0.05 mag. The correction

away from solar metallicity to the cluster metallicity, $[\text{Fe}/\text{H}] = -0.21 \pm 0.10$ (Barrado y Navascués et al. 2001a), would require a shift in distance modulus of -0.13 ± 0.06 mag (Pinsonneault et al. 1998). Besides this possible systematic shift due to metallicity, the fit between our cluster fiducial sequence and the Pinsonneault et al. fiducial is excellent, with a residual of -0.033 ± 0.033 mag (fitting error) ± 0.087 mag (error in fiducial points) $= -0.033 \pm 0.093$ if we use the three M35 fiducial points within the Pinsonneault et al. fitting range. Expanding the fit to the two points immediately outside this fitting range, and giving these points half the weight of the central three points, we find a residual of $-0.051 \pm 0.027 \pm 0.075$ mag $= -0.051 \pm 0.080$. Main sequence fitting of the Pinsonneault et al. sequence to our 0.9m data for M35 supports our cluster distance modulus within ± 0.09 mag, with perhaps marginal evidence that the cluster distance modulus is slightly greater than the one we employ, $(m - M)_V = 10.15 + (0.03 \text{ to } 0.05 \text{ main sequence offset}) + (-0.13 \pm 0.06 \text{ possible metallicity offset})$.

Before proceeding to compare M35’s fiducial main sequence to stellar evolution models we first compare it to the fiducial main sequence presented by BSBM, which they derived primarily by fitting a sequence to field star photometry with accurate parallaxes presented by Leggett (1992), and secondarily, for the bright stars, by fitting the photometry of Sung & Bessell (1999). This comparison is plotted in Figure 6, where we use our adopted distance modulus and reddening to convert both observed fiducial sequences to a common absolute magnitude and dereddened $V - I$. Our fiducial sequence is ~ 0.05 mag redder in $V - I$ for $M_V \geq 8$, and significantly redder at the faintest magnitudes, corresponding to a shift of 0.20 mag at $M_V = 14$. Alternatively, our fiducial sequence is brighter than BSBM’s fiducial sequence, with a systematically increasing luminosity difference for the faintest stars. It is unclear what the source of this color or luminosity offset could be. The BSBM fiducial is drawn from a heterogeneous local field stellar sample, so perhaps this heterogeneity is the cause of the difference. Yet on average their field stars should have the same or greater metallicity than M35, which would produce an offset in the opposite direction. Also, as discussed earlier, any systematic due to extrapolating our color terms for the reddest stars would not help, since the expected correction would only make our faintest main sequence stars redder.

In Figure 7 we compare the fiducial main sequences of M35, NGC 188 (WOCS1), NGC 2420 (von Hippel & Gilmore 2000), and NGC 2477 (derived from von Hippel et al. 1996). The latter two cluster sequences are based on HST photometry, whereas the former two are based on WIYN photometry, though the NGC 188 data were directly calibrated at WIYN while these M35 data were calibrated with 0.9m photometry. All four clusters have the potential for systematic photometry errors among the reddest stars, due to the same problem with insufficient standards for $V - I \gtrsim 2$. The HST calibrations,

for instance, degrade past $V - I = 1.5$ (Holtzman et al. 1995). Hopefully, however, these systematics manifest themselves differently in the different instruments and the range in the photometry is an indication of their reliability. In addition, there are slight differences in metallicity, with $[\text{Fe}/\text{H}](\text{NGC } 2420) \approx -0.4$, $[\text{Fe}/\text{H}](\text{M35}) \approx -0.2$, and $[\text{Fe}/\text{H}](\text{NGC } 188) \approx [\text{Fe}/\text{H}](\text{NGC } 2477) \approx 0.0$. These small metallicity differences only correspond to small color or luminosity shifts, with a deficiency of 0.2 dex in $[\text{Fe}/\text{H}]$ corresponding to a shift blueward by $B - V \approx 0.005\text{--}0.04$ and $V - I \approx 0.04\text{--}0.07$, depending on the luminosity. After incorporating the effects of metallicity, the lower main sequence of M35 appears to be redder than the other clusters by $\Delta(V - I) = 0.2$ mag. Although this offset is most likely due to the uncertainties in the color transformations, we do not correct for it, since we don’t know which clusters are in error. Fortunately, the differences in sequences are minor compared to the current uncertainties in the stellar evolution models.

3.4. Comparison to Stellar Models

We now compare our fiducial sequences to stellar models by four groups. Readers should keep in mind that all groups acknowledge difficulties matching observations below $\sim 0.4 M_\odot$ (corresponding to $T_{\text{eff}} \approx 4000$ K, $B - V \approx 1.3$, and $V - I \approx 2.0$). The reasons for difficulties with the cool stars are many: the fundamental problem of convection, uncertainties in the opacities, the equation of state, and creating reliable model atmospheres. For instance, the incomplete treatment of convection and uncertainties in the opacities, particularly molecular opacities, affect model radii. Without reliable model radii, it becomes impossible to create reliable color- T_{eff} transformations. With these difficulties in mind, our comparisons are meant to help quantify the level of mismatch between theory and observation in two common (BV and VI) broad-band CMDs, and to help observers choose appropriate models and estimate errors when studying these low mass stars.

Figure 8a compares the VI cluster fiducials for M35 and NGC 188 to solar metallicity stellar isochrones from Baraffe et al. (1998). The small subsolar metallicity for M35 corresponds to a shift in the models which makes them nearly match M35 above $0.45 M_\odot$, but exacerbates the difference between the models and the clusters below $0.45 M_\odot$. The 158 Myr and the 6.3 Gyr models are the models closest in age to M35 (150 Myr, Deliyannis et al. 2002) and NGC 188 (7 ± 0.7 Gyr, Sarajedini et al. 1999), respectively. Mass values in solar units are indicated along the 158 Myr isochrone. According to these models, our M35 photometry extends down to $\sim 0.10 M_\odot$. Both the 158 Myr and 6.3 Gyr isochrones are too blue for stars less massive than $\sim 0.45 M_\odot$. The slope of the fiducial main sequences and the model isochrones begin to diverge somewhat earlier, between $M_V = 8$ and 9. In

Figure 8b updated, unpublished models kindly supplied by I. Baraffe are compared to the same data. These unpublished models are identical to those of Baraffe et al. (1998) except that the TiO line list from Schwenke (1998) instead of Jorgensen (1994) was used (see also section 3.1 of Chabrier et al. 2001 for details). These models appear to be an improvement: the color discrepancy with the lowest mass stars is reduced by a factor of approximately two.

Figure 9a compares the BV M35 fiducial sequence to $[\text{Fe}/\text{H}] = -0.3$ stellar isochrones from Siess, Dufour, & Forestini (2000). Two separate color transformations for the isochrone appropriate to M35 are plotted, one compiled by Siess, Forestini, & Dougados (1997) and the other from Kenyon & Hartmann (1995). Figure 9b provides the same comparison in the VI CMD, this time also including NGC 188 and an appropriate isochrone. To approximately the same degree as the updated Baraffe et al. models, the Siess et al. models are too blue starting at $M_V = 8-9$, and we see that the problem is not limited to VI photometry.

Figures 10a and 10b provide similar comparisons to the Girardi et al. (2000) isochrones, for which the deviation between the models and cluster fiducials are more pronounced, especially in the VI CMD. For the last model comparison, Figures 11a and 11b compare the cluster fiducials to Yonsei-Yale (Yi et al. 2001) isochrones. Since Yi et al. provide an interpolation tool with their isochrones, we created a 150 Myr, $[\text{Fe}/\text{H}] = -0.2$ isochrone to precisely match M35’s parameters, and a 7 Gyr, $[\text{Fe}/\text{H}] = 0$ isochrone to precisely match NGC 188’s parameters. Two different color calibrations are presented—one (indicated by a solid line) by Lejeune, Cuisinier, & Buser (1998) and the other (indicated by a dotted line) an updated version of the transformations of Green, Demarque, & King (1987). The Yonsei-Yale models are also too blue for much of the lower main sequence in the BV CMD, but surprisingly are too red in the VI CMD, for $V - I \gtrsim 2.8$. The constant slope at the lower mass end, however, is an indication that these models are extrapolating at least some of the physics applicable for intermediate mass stars into the low mass regime, in this case the equation of state is extrapolated below $0.45 M_\odot$ (P. Demarque, private communication). To be fair, the Girardi et al. and the Yi et al. models were not designed for this very low mass range, and we present them along with the Baraffe et al. and Siess et al. models, which were designed for this mass range, only to present a more complete comparison with current stellar models.

In essentially all cluster-to-model comparisons the models are too blue in both $B - V$ and $V - I$ for stars less massive than $\sim 0.4 M_\odot$. It is unlikely that errors in our photometric calibration cause this discrepancy since the lower main sequence we derive for M35 is consistent with the lower main sequences for three other star clusters and since the likely

systematic error in our color terms would only make the actual stars 0.1 to 0.2 mag redder, increasing the discrepancies with the models. At least part of the cluster-to-model mismatch appears to be underestimated opacity in the bluer bandpasses, with the amount of missing opacity increasing toward the blue ($B - V$ already includes the excess V -band opacity apparent in $V - I$). More generally, at low temperatures, both the model radii and the color transformations between the theoretical L - T_{eff} plane and the observational plane are still uncertain, due to the unphysical parameterization of convection (mixing length theory) and deficiencies in current model atmospheres (particularly molecular transition data), respectively. We look forward to developments in these theories and more sophisticated models that fully treat radiative hydrodynamics.

3.5. Luminosity Function

The steps used to derive the VI fiducial sequence from the subtracted VI CMD density map were essentially the same as deriving the cluster luminosity function. The process of shifting the comparison field slightly to correct for its lower reddening, smoothing the CMDs, subtracting the smoothed control field CMD from the cluster field CMD, and identifying and statistically validating the location of the cluster main sequence, leads us to the point where we need only extract the number of stars in the differenced CMD along the main sequence. The only parameter in question for the luminosity function was the appropriate width along the main sequence. In theory the best extraction width might vary as a function of magnitude since the photometric errors increase toward the bottom of the CMD and since the main sequence slope changes with luminosity. In practice, because the comparison and cluster fields were closely matched in the properties of the field stars and the photometric depth, the width of the extraction window did not matter, at least within a reasonable range. The insensitivity of the total star counts in the LF (from $19.82 \leq V \leq 24.62$) versus the extraction window width (Figure 4) demonstrates this point. Once the window width reached 0.29 mag (± 0.14 mag around the fiducial sequence) the total number of stars in the LF remained constant, at 47. In order to test for any signature due to equal mass binary main sequence stars at 0.75 mag above the main sequence, we chose an extraction width of 0.15 mag (± 0.07 mag) around a locus offset by -0.75 mag. This extraction width kept the equal mass binary window from overlapping the main sequence extraction window. One untreated systematic in this procedure was the effect of removing real cluster stars by using a conservative stellarity index. Fortunately, as Figure 1 illustrates, real cluster stars may be missed only for $I \leq 22$, which is beyond the limit of the main sequence luminosity function we extract (to $V = 24.62$).

As a final nuance to the derived cluster LF, we identify a small number of objects in the control field as possible cluster stars, consistent with star counts from the wide-field 0.9m photometry (derived from the data of Deliyannis et al. 2002) at brighter magnitudes ($V \geq 18$) where we find the cluster density in the control field may not diminish altogether to zero, but rather appears to have dropped to $10 \pm 10\%$ of the central value. This possible small contamination, with a significance of only 1σ , does not include systematic effects such as mass segregation, which would increase the relative numbers of the faintest stars at greater cluster radii. Our control field thus may oversubtract cluster stars by $\sim 10\%$ and our LFs may therefore slightly underestimate the true cluster LF in this central field. Since we are not making detailed comparisons among our derived LF and the LFs of other clusters, or attempting to recover M35’s IMF, this possible and slight underestimate of M35’s LF does not pose a problem in our analysis. Instead, we use M35’s LF to demonstrate the reality of our cluster fiducial sequence by showing that we have actually found cluster stars along this sequence and to demonstrate that the cluster contains very low mass stars to the limit of our photometry, just slightly above the brown dwarf regime.

The differential M35 LF, binned in 0.5 mag intervals, is presented in Figure 12a, along with error bars derived from the Poisson counting statistics of the cluster and comparison field. The presence of cluster stars is most convincing at the faint end, which fortunately allows us to define the fiducial sequence and compare it to stellar models, above. Figure 12b presents the cumulative luminosity function for M35 along with the cumulative LF for the cluster equal mass binaries. The fraction of binaries among the low mass stars in this field is low or even zero, even though binaries are abundant ($\sim 35\%$, Sung & Bessell 1999) among the high mass cluster stars. The number of cluster stars continues to increase to the LF limit, at $V = 24.6$. In addition, Figure 12b also presents the mapping between V -band magnitude and mass in solar units at $[\text{Fe}/\text{H}] = 0.0$ for our assumed cluster distance and each of the stellar isochrones discussed above. This is presented in lieu of mass functions for each stellar isochrone set, which would anyway have too few stars to yield much information. Clearly the different theoretical mass-luminosity relations, at least in M_V , differ by too much for reliable mass estimates in this mass range.

The low number of stars in our field and our focus on the fiducial main sequence rather than the LF meant that a detailed completeness study to correct the cluster LF was not warranted. Nonetheless, we are able to reliably and conservatively estimate completeness from the signal-to-noise as a function of depth derived from past artificial star experiments with nearly identical data taken at WIYN with the same detector and filters, under similar and very low levels of crowding and sky illumination, but under poorer seeing conditions (WOCS1). Based on these earlier tests, we estimate that the cluster LF is 90% complete at $V = 24.4$, just before the faint end of the extracted LF. For comparison, 0.4 mag beyond

the end of the extracted LF, but nearly a magnitude above the bottom of the *VI* CMD, at $V = 25.2$, we estimate completeness to be 50%.

3.6. The Observed Lower Mass Limit

M35 contains stars to the limit of the extracted main sequence, at $M \approx 0.10\text{--}0.15 M_{\odot}$ (using masses derived from the Baraffe et al. 1998 models). This suggests that M35 may harbor a large number of brown dwarfs. Where does the brown dwarf region in M35 start? As demonstrated in Figure 12b, estimating this magnitude depends on which stellar isochrone set one adopts. As an example, we adopt the results of Chabrier, Baraffe, & Plez (1996), who find that the H-burning minimum mass for solar metallicity is $\sim 0.070 M_{\odot}$. (The slight sub-solar metallicity for M35 ($[\text{Fe}/\text{H}] = -0.2$) should increase this minimum mass by a small amount, $\sim 0.002 M_{\odot}$ (Cabrier et al. 1996), though we ignore this small offset in calculating the H-burning limit.) Interpolating values from table 1 of Chabrier et al. for the cluster age of 150 Myr yields the following properties for an H-burning minimum mass object: $T_{\text{eff}} = 2660$ K, $\log(L/L_{\odot}) = -3.02$, $M_V = 15.8$, $M_I = 12.6$, and $M_K = 9.3$. With the *V*-band cluster distance modulus of 10.15 and $E(B - V) = 0.2$ this is just beyond the limit of our observations, at $V \approx 26$, corresponding to $I \approx 22.7$ and $K \approx 19.1$. Particularly in the near-IR such observations are now readily obtainable even on 4m class telescopes.

4. White Dwarfs

Reimers & Koester (1988a,b) obtained spectra of candidate white dwarfs (WDs) identified in M35 by Romanishin & Angel (1981) in a series of papers meant to ascertain the upper mass limit for the formation of WDs and to constrain the WD initial-final mass relation. With an age of ~ 150 Myr, M35 has a turn-off mass of $\sim 3.75 M_{\odot}$ (e.g., from the overshooting models of Girardi et al. 2000), and is certainly expected to have produced white dwarfs. Reimers & Koester identified two objects, which they call N2168-3 and N2168-4, as white dwarfs that are likely cluster members with $T_{\text{eff}} = 37500$ and 44000 K, both with masses $= 0.7 \pm 0.1 M_{\odot}$, and cooling ages of $\sim 1.5 \times 10^7$ yr. They reported *V*-band magnitudes of 20.24 and 20.05 for these two objects. Their cooling ages and photometry are consistent with objects which left the cluster main sequence when the cluster was $\sim 80\%$ its current age. Their mass estimate is perhaps 1σ lower than their age derivation, more modern WD models, and the cluster age would imply.

While the Reimers & Koester WDs were not in our field, we have found a new candidate cluster WD at $RA = 06^h09^m06^s.2$ and $Dec = 24^\circ 19' 25''$ (J2000). This candidate, along with three other blue objects from the control field, can be found in figures 2a through 2d near $B - V \approx V - I \approx 0.0$. A closer look at these four candidate WDs are presented in Figures 13a, 13b, and 14, where they are compared to WD cooling tracks of Althaus & Benvenuto (1997, 1998) for H- and He-atmospheres and Wood (1992, and references therein; with colors derived from interpolating in the tables of Bergeron, Wesemael, & Beauchamp 1995) for H-atmospheres, respectively. In all three figures the model cooling tracks with the highest and lowest masses (in solar units) are labeled, as are illustrative ages (in Gyr) along the tracks. The listed ages are the total WD age, derived from the addition of the WD cooling ages from the above-referenced models and our determination of the precursor ages. The precursor ages were derived by converting WD masses used in the tracks to zero age main sequence masses using the new initial-final mass relation of Weidemann (2000), along with stellar evolutionary time scales up to the tip of the asymptotic giant branch derived from interpolations of the Girardi et al. (2000) solar metallicity models, including convective overshoot. We chose the Girardi et al. models because of their fine grid in mass and age for the range of relevance here, though we checked them against time scales for models with the same masses from Hurley, Pols, & Tout (2000) and Yi et al. (2001), and the differences in precursor ages were always $\leq 10\%$. A $0.7 M_\odot$ WD would have been a $3.17 M_\odot$ star on the main sequence with a pre-WD lifetime of 0.410 Gyr. A $1.0 M_\odot$ WD would have been a $6.71 M_\odot$ star on the main sequence with a pre-WD lifetime of < 0.063 Gyr. Uncertainties in these short precursor ages of $\leq 10\%$ have little effect (< 6 Myr) on the derived age for the highest mass WDs expected to be the oldest in the cluster.

The blue objects from the control field are highly unlikely to belong to the cluster due to both the very low number of cluster stars at this location and due to the implied ages of ≥ 0.6 Gyr. These objects may be field WDs, in which case they are most likely in the background and therefore belong on lower mass tracks and are older, or they may be background quasars. The single blue object in the M35 central field with $V = 21.36 \pm 0.01$ is a good candidate WD, based on the rarity of other stars and blue compact galaxies at this magnitude, although its exact interpretation if it is a cluster WD is unclear. As a cluster WD, according to the H-atmosphere cooling tracks of Althaus & Benvenuto (Figure 13a), it would have a mass of $1.05 \pm 0.05 M_\odot$ and an age of 0.21–0.26 Gyr ($\pm 1\sigma$ range), which is certainly possible, but the lower limit is formally more than 4σ higher than the cluster age derived by Deliyannis et al. (2002) and WDs this massive are rare. The He-atmosphere cooling tracks of Althaus & Benvenuto (Figure 13b) decrease the age slightly, to 0.19–0.22 Gyr, bringing them into closer consistency (but still formally off by 3σ) with the isochrone age, although the mass does not change appreciably. Although WDs this massive are rare

in the field ($\sim 1\%$), they are not as rare in young clusters and the apparent high mass of the WD candidate is sensible for the cluster age and turn-off mass. According to the Weidemann (2000) initial-final mass relation, this object would have been a $\sim 7 M_{\odot}$ star on the main sequence, making it potentially important in the determination of the upper mass limit for WD creation. On the other hand, interpreting this object with the H-atmosphere cooling tracks of Wood (1992), yields a WD mass of $0.67\text{--}0.78 M_{\odot}$ and an age of $0.42\text{--}0.83$ Gyr. We do not know the source of the inconsistency between Althaus & Benvenuto on the one hand and Wood and Bergeron et al. (the source of the temperature-color calibration) on the other hand. To further test the WD models, as well as determine if the candidate cluster WD is a *bona fide* cluster WD, follow-up spectroscopy is required. If the object turns out to be a cluster WD then the nature of its atmosphere (H or He) as well as its surface gravity (if an H-atmosphere WD) will yield its mass and further test the WD models, while at the same time intercalibrating the WD and main sequence models. The differences in the derived main sequence and WD ages could be due to real problems in stellar evolution of intermediate mass stars, where age depends sensitively on the degree of mixing in convective cores. Accurate parameters for this star and data able to discern its possible cluster membership would be particularly valuable.

5. Conclusion

We obtained deep *BVI* observations of M35 and a nearby comparison field with the WIYN 3.5m telescope under non-photometric but excellent seeing conditions. We calibrated the data against shallower 0.9m data (from Deliyannis et al. 2002), achieving a photometric accuracy of approximately 0.02 mag. These deep observations display the lower main sequence in the *BV* and *VI* CMDs down to $V = 23.3$ and 24.6 , respectively. At these faint magnitudes the background Galactic field stars are far more numerous than the cluster stars, yet by using a smoothing technique (Silverman 1986) and CMD density distribution subtraction we were able to recover the cluster fiducial main sequence and luminosity function to $V = 24.6$. We find the location of the M35 main sequence in these CMDs to be consistent with earlier work on other open clusters, specifically NGC 188 (WOCS1), NGC 2420 (von Hippel & Gilmore 2000), and NGC 2477 (von Hippel et al. 1996). On comparing these open cluster fiducial sequences to stellar models by Baraffe et al. (1998), Siess et al. (2000), Girardi et al. (2000), and Yi et al. (2001) we find that the models are too blue in both $B - V$ and $V - I$ for stars less massive than $\sim 0.4 M_{\odot}$. At least part of the problem appears to be underestimated opacity in the bluer bandpasses, with the amount of missing opacity increasing toward the blue.

M35 contains stars to the limit of the extracted main sequence, at $M \approx 0.10\text{--}0.15\ M_{\odot}$, suggesting that M35 may harbor a large number of brown dwarfs. These brown dwarfs should be easy targets for sensitive near-IR instrumentation now being mounted on 8–10m telescopes. In fact, imaging observations of only one hour in K would allow one to obtain $S/N = 30$ photometry 1 magnitude fainter than the brown dwarf limit in this cluster.

We also identify a new candidate white dwarf in M35 at $V = 21.36 \pm 0.01$. Depending on which WD models are used in interpreting this object, it is either a very high mass WD ($1.05 \pm 0.05\ M_{\odot}$) somewhat ($3\text{--}4\sigma$) older than our best isochrone age (150 Myr), or it is a modestly massive WD ($0.67\text{--}0.78\ M_{\odot}$) much too old (0.42–0.83 Gyr) to belong to the cluster. Follow-up spectroscopy is required to resolve this issue.

T. von Hippel would like to thank Isabelle Baraffe, Pierre Demarque, Karl Gebhardt, and Don Winget for helpful discussions; Isabelle Baraffe, Gilles Chabrier, France Allard, and Peter Hauschildt for their unpublished models; and Karl Gebhardt for the software used for the field star subtraction procedure. We also thank an anonymous referee for a number of suggestions that improved the rigor and clarity of the paper. A. Sarajedini and T. von Hippel gratefully acknowledge support for this work from NSF grants AST-9819768 and AST-0196212, and C. P. Deliyannis gratefully acknowledges support from NSF grant AST-9812735.

REFERENCES

- Althaus, L. G., & Benvenuto, O. G. 1997, *ApJ*, 477, 313
- Althaus, L. G., & Benvenuto, O. G. 1998, *MNRAS*, 296, 206
- Baraffe, I., Chabrier, G., Allard, F., & Hauschildt, P. H. 1998, *A&A*, 337, 403
- Barrado y Navascués, D., Deliyannis, C. P., & Stauffer, J. R. 2001a, *ApJ*, 549, 452
- Barrado y Navascués, D., Stauffer, J. R., Bouvier, J., & Martín, E. L. 2001b, *ApJ*, 546, 1006
- Bergeron, P., Wesemael, F., & Beauchamp, A. 1995, *PASP*, 107, 1047
- Cardelli, J. A., Clayton, G. C., & Mathis, J. S. 1989, *ApJ*, 345, 245
- Chabrier, G., Baraffe, I., Allard, F., & Hauschildt, P. 2000, *ApJ*, 542, 464
- Chabrier, G., Baraffe, I., & Plez, B. 1996, *ApJ*, 459, L91
- Cudworth, K. M. 1971, *AJ*, 76, 475
- Deliyannis, C. P., Steinhauer, A., Sarrazine, A. R., Sarajedini, A., Hainline, L. J., Bailyn, C. D., Platais, I., Kozhurina-Platais, V., & von Hippel, T. 2002, in preparation for *AJ*
- Ebbighausen, E. G. 1942, *AJ*, 50, 1
- Erro, B. I. 1969, *Tonantzintla Tacubaya*, 5, 89
- Gebhardt, K., Pryor, C., Williams, T. B., & Hesser, J. E. 1995, *AJ*, 110, 1699
- Gebhardt, K., et al. 1996, *AJ*, 112, 105
- Girardi, L., Bressan, A., Bertelli, G., & Chiosi, C. 2000, *A&AS*, 141, 371
- Green, E. M., Demarque, P., & King, C. R. 1987, *The Revised Yale Isochrones and Luminosity Functions* (New Haven: Yale Univ. Obs.)
- Holtzman, J. A., Burrows, C. J., Casertano, S., Hester, J. J., Watson, A. M., & Worthy, G. S. 1995, *PASP*, 107, 1065
- Hurley, J. R., Pols, O. R., & Tout, C. A. 2000, *MNRAS*, 315, 543
- Johnson, H. L. 1966, *ARA&A*, 4, 193
- Jorgensen, U. G. 1994, *A&A*, 284, 179
- Kenyon, S. J. & Hartmann, L. 1995, *ApJS*, 101, 117
- Landolt, A. U. 1983, *AJ*, 88, 439
- Landolt, A. U. 1992, *AJ*, 104, 340
- Lavdovskij, V. V. 1961 *Trans. Pulkovo Astr. Obs.*, 73, 5

- Lejeune, Th., Cuisinier, F., & Buser, R. 1998, *A&A*, 130, 65
- Leonard, P. J. T., & Merritt, D. 1989, *ApJ*, 339, 195
- McArthur, B., Benedict, G. F., Jefferys, W. H., & Nelan, E. 1997, in *The 1997 HST Calibration Workshop with a New Generation of Instruments*, ed. S. Casertano, R. Jedrzejewski, C. D. Keyes, & M. Stevens (Baltimore: Space Telescope Science Institute), 472
- McNamara, B. J., & Sekiguchi, K. 1986a, *AJ*, 91, 557
- McNamara, B. J., & Sekiguchi, K. 1986b, *ApJ*, 310, 613
- Maeder, A., & Mermilliod, J. C. 1981, *A&A*, 93, 136
- Mathieu, R. 1983, Ph.D. Thesis, UC Berkeley
- Meurers, J., & Schwarz, A. 1960, *Veroff. Univ. Stern. Bonn*, No. 53
- Pickles, A. J. 1998, *PASP*, 110, 863
- Pinsonneault, M. H., Stauffer, J., Soderblom, D. R., King, J. R., & Hanson, R. B. 1998, *ApJ*, 504, 170
- Reid, I. N., & Majewski, S. R. 1993, *ApJ*, 409, 635
- Reimers, D., & Koester, D. 1988a, *A&A*, 202, 77
- Reimers, D., & Koester, D. 1988b, *Messenger*, 54, 47
- Romanishin, W., & Angel, J. R. P. 1981, *ApJ*, 235, 992
- Salpeter, E. E. 1955, *ApJ*, 121, 161
- Sarajedini, A., von Hippel, T., Kozhurina-Platais, V., & Demarque, P. 1999, *AJ*, 118, 2894
- Schwenke, D. W. 1998, *Faraday Discuss.*, 109, 321
- Siess, L., Dufour, E., & Forestini, M. 2000, *A&A*, 358, 593
- Siess, L., Forestini, M., & Dougados, C. 1997, *A&A*, 324, 556
- Silverman, B. W. 1986, *Density Estimation for Statistics and Data Analysis*, (New York: Chapman and Hall)
- Stetson, P. B. 1994, *PASP*, 106, 250
- Sung, H., & Bessell, M. S. 1999, *MNRAS*, 306, 361
- Sung, H., & Lee, S.-W. 1992, *JKAS*, 25, 91
- von Hippel, T., & Gilmore, G. 2000, *AJ*, 120, 1384
- von Hippel, T., Gilmore, G., Tanvir, N., Robinson, D., & Jones, D. H. P. 1996, *AJ*, 112, 192

von Hippel, T., & Sarajedini, A. 1998, *AJ*, 116, 1789

Weidemann, V. 2000, *A&A*, 363, 647

Wood, M.A. 1992, *ApJ*, 386, 539

Yi, S., Demarque, P., Kim, Y.-C., Lee, Y.-W., Ree, C. H., Lejeune, Th., & Barnes, S. 2001, *ApJS*, 136, 417

Fig. 1.— I -band magnitude versus stellarity index for the M35 central field (solid circles) and the control field (open circles). The control field points have been shifted down by 0.1 and to the right by 1.0 mag for visibility. The stellarity index cut of 0.95, the threshold for inclusion of the objects in the CMDs and subsequent analyses, is indicated for both fields.

Fig. 2.— $B - V$ versus V CMD for (a) the cluster central field and (b) the control field. Typical error bars for cluster main sequence stars are plotted along the right. The fiducial main sequence is also indicated by the solid line. $V - I$ versus V CMD for (c) the cluster central field and (d) the control field.

Fig. 3.— The smoothed version of the VI CMD for the (a) cluster central field and (b) the comparison field with a smoothing kernel of 0.10 mag. The horizontal axes are $V - I$ color from 0.0 to 4.5 and the vertical axes are V magnitude from 15 to 26. The difference CMD (c) exhibits a subtle but clear main sequence just above the solid white line, itself the fitted fiducial offset 0.3 mag fainter for display purposes. Subtraction noise throughout the field star region is evident, though the net star number there is close to zero.

Fig. 4.— The cumulative star count in the extracted VI luminosity function as a function of the width of the $V - I$ extraction window. The solid line running through open circles presents the cumulative star count for an extraction window centered on our initial cluster fiducial sequence. From left to right the curves present cumulative star counts for windows shifted by $V - I = +0.025, 0.000, +0.050, -0.025, +0.075, -0.050, +0.100, -0.075, +0.125, -0.100$, and -0.125 mag, where positive shifts are toward the red. The fiducial offset by $V - I = +0.025$ is the one we adopt as the best fit. After a window width of 0.29 mag (± 0.14 mag around the fiducial sequence) the number of stars remains essentially constant for our chosen and nearby fiducial sequences, demonstrating the stability of the CMD subtraction technique.

Fig. 5.— Comparison of the upper portion of the fiducial sequence to the Hipparcos-based fiducial sequence derived by Pinsonneault et al. (1998) in the dereddened VI CMD, indicating good consistency with our adopted cluster distance and reddening. The dashed line extends across the region of the Pinsonneault et al. calibration and the error bars are estimated uncertainties in the individual fiducial points.

Fig. 6.— Comparison between our M35 fiducial main sequence and the adopted main sequence of Barrado y Navascués et al. (2001b), itself a combination of bright M35 stars from Sung & Bessell (1999) and faint solar neighborhood stars from Leggett (1992).

Fig. 7.— Comparison between the M35 fiducial main sequence and the fiducial main sequences of the older open clusters NGC 188, NGC 2420, and NGC 2477. The portion of the M35 fiducial derived from the Kitt Peak 0.9m and WIYN data is indicated by a

dotted line and a solid line connecting the filled circle symbols, respectively. NGC 188 is plotted as open circles along a solid line.

Fig. 8.— (a) Comparison between the M35 and NGC 188 main sequences and the solar metallicity models of Baraffe et al. (1998). Stellar models for 158 Myr and 6.3 Gyr are indicated, as are a few representative mass values in solar units along the 158 Myr isochrone. (b) Similar to a but the Baraffe et al. models employ an updated TiO line list from Schwenke (1998).

Fig. 9.— Comparison between the M35 main sequence in the (a) dereddened *BV* CMD with Siess et al. (2000) isochrones, using either the color transformations of Siess et al. (1997, full line) or Kenyon & Hartmann (1995, dashed line). The same comparison in the (b) dereddened *VI* CMD, now including NGC 188 and a comparably aged set of isochrones.

Fig. 10.— Similar to Figures 9a and 9b, but now comparing the cluster fiducials to solar metallicity Girardi et al. (2000) isochrones.

Fig. 11.— Similar to Figures 9a and 9b, but now comparing the cluster fiducials to Yi et al. (2001) isochrones. For both clusters two isochrones are plotted for two different color transformations. The dotted line indicates the transformation derived by Green et al. (1987) and the solid line the transformation derived by Lejeune et al. (1998).

Fig. 12.— The (a) differential and (b) cumulative luminosity function extracted from the *VI* CMD. The differential luminosity function is plotted with error bars derived from the Poisson statistics of the subtraction process. The cumulative LF for both the main sequence stars and any possible equal mass binary signature are plotted, along with mass values from various models. The symbols to the left of the mass values indicate their origin, and are B = Baraffe et al. (1998), S_K = Siess et al. (2000) employing the Kenyon & Hartmann (1995) color transformation, S = Siess et al. (2000) employing the Siess et al. (1997) color transformation, G = Girardi et al. (2000), and Y = Yi et al. (2001). Incompleteness corrections, which amount to $\sim 10\%$ at the faint end of the LF, are not included.

Fig. 13.— The candidate cluster WD (square symbol) from the central field and candidate field WDs (circle symbols) from the control field compared to (a) H-atmosphere and (b) He-atmosphere WD cooling tracks from Althaus & Benvenuto (1997, 1998). The highest and lowest mass cooling tracks are marked with their mass in solar units. Total WD ages in Gyr along some of the cooling tracks are also indicated.

Fig. 14.— Same as Figure 13a, but for Wood (1992) cooling tracks, incorporating the T_{eff} -color transformations of Bergeron et al. (1995).

Table 1. Calibration to Landolt System

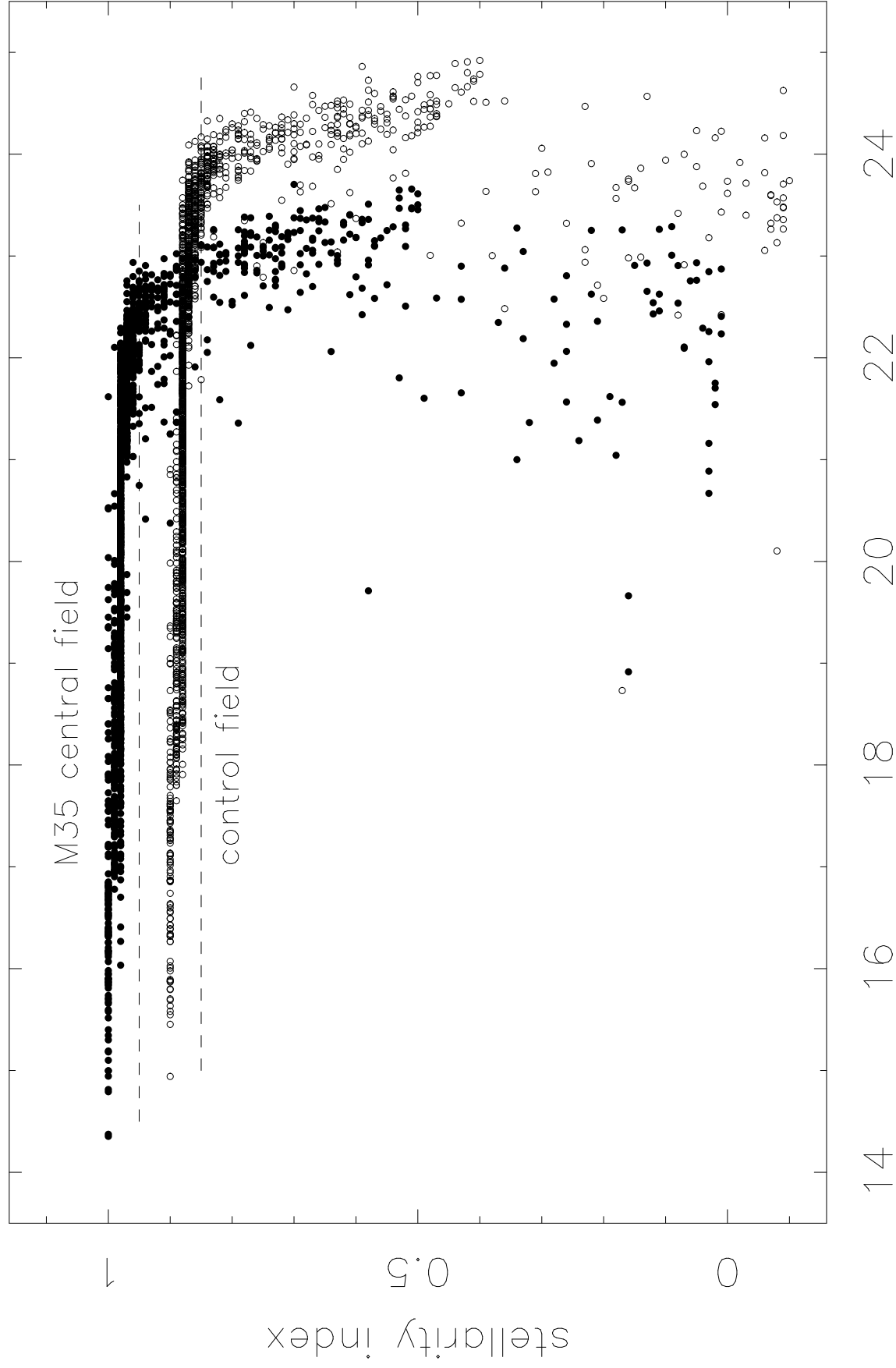
filter (1)	frames (2)	stars (3)	zeropt (4)	err (5)	airmass (6)	err (7)	color (8)	err (9)
B	7	63	3.4567	0.0149	0.2235	0.0114	-0.0814	0.0035
$V=f(B - V)$	7	65	3.2405	0.0134	0.1179	0.0102	0.0107	0.0031
$V=f(V - I)$	7	67	3.2413	0.0137	0.1167	0.0104	0.0111	0.0029
I	7	77	3.8970	0.0121	0.0448	0.0090	-0.0122	0.0024

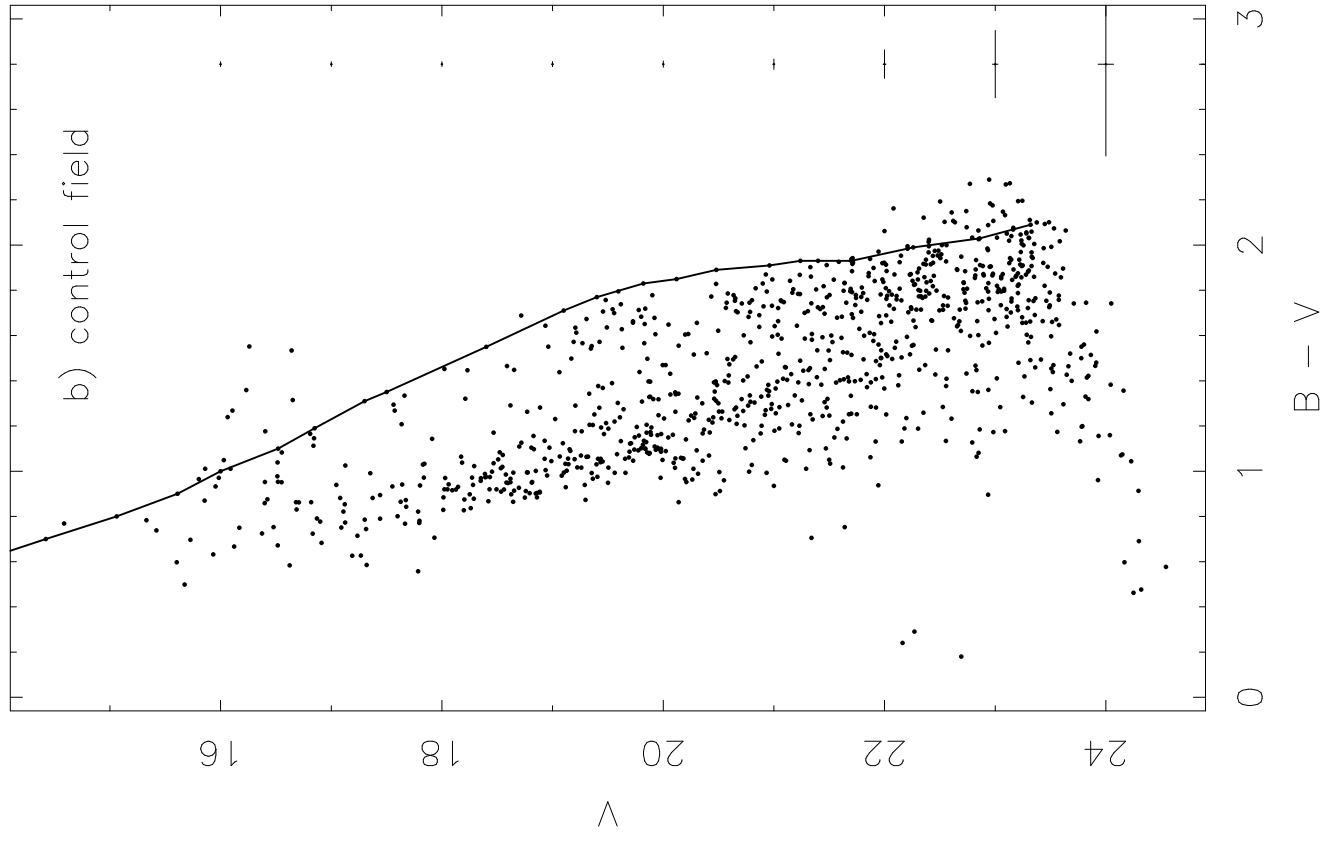
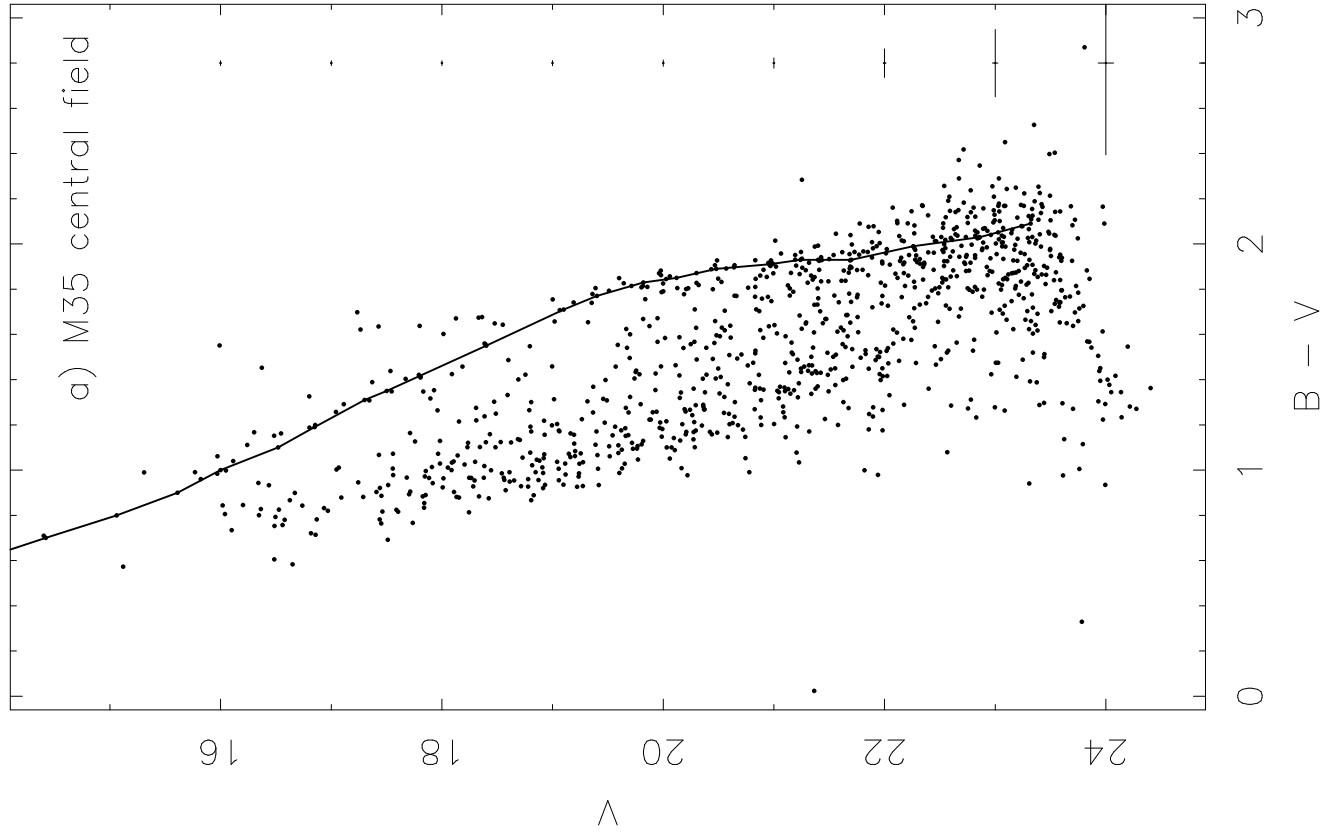
Table 2. *BV* Fiducial Main Sequence

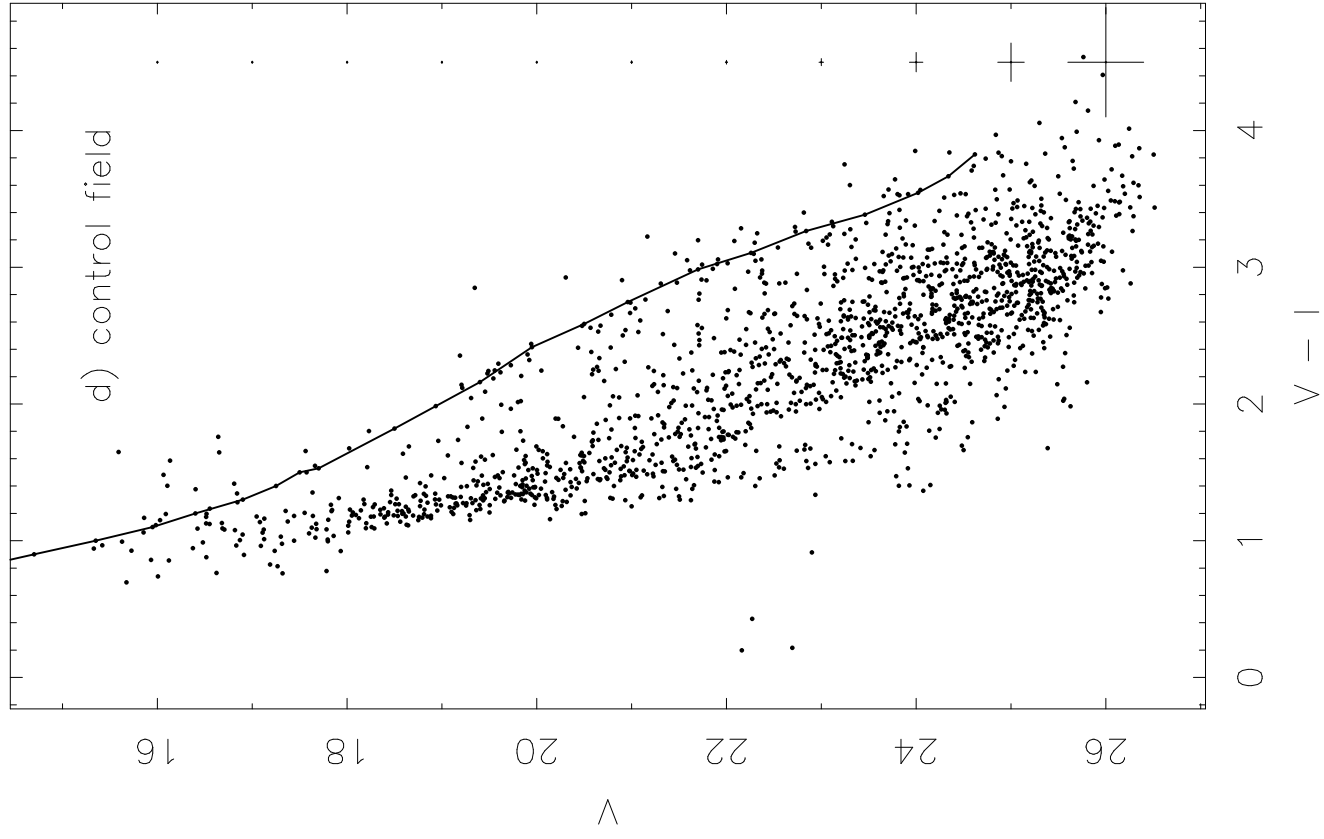
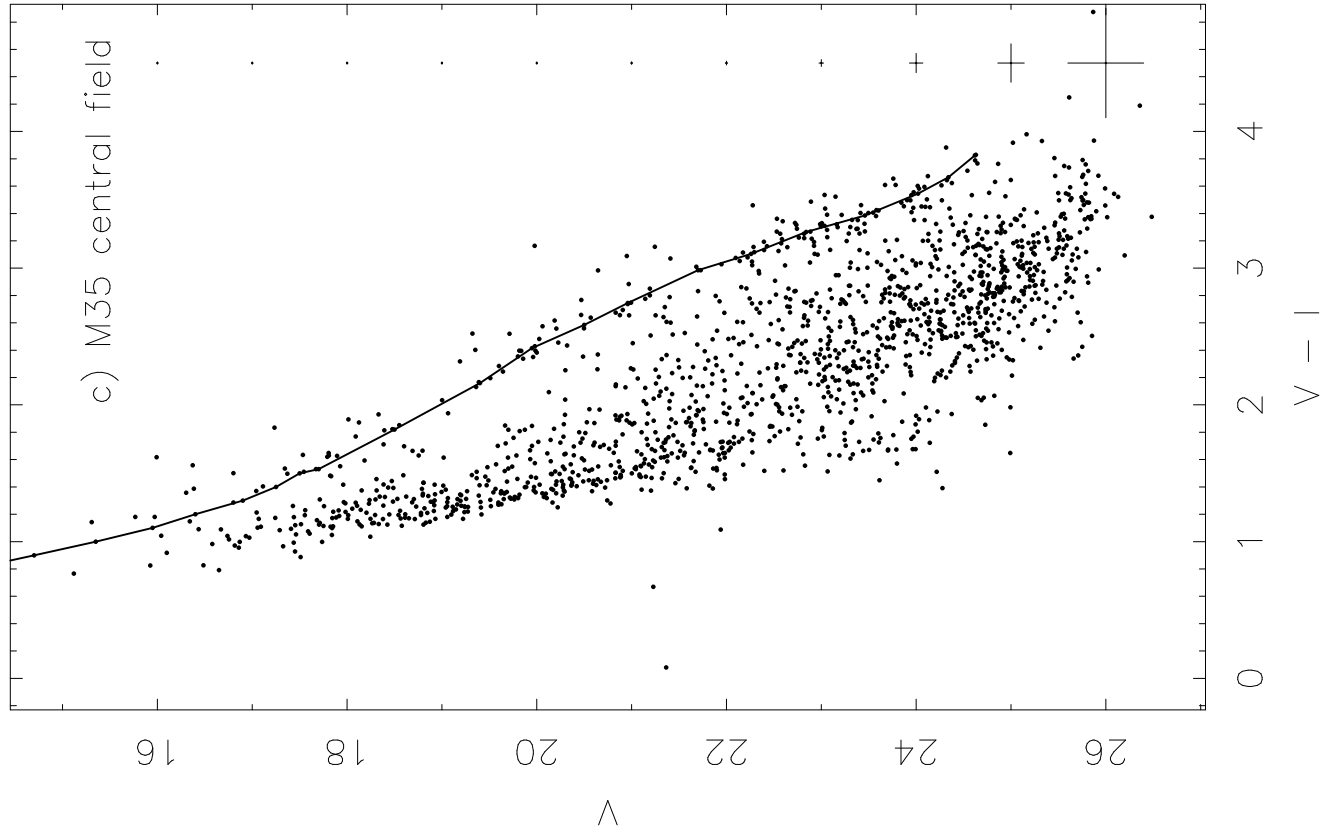
$B - V$	V
(1)	(2)
0.15	11.31
0.2	11.72
0.3	12.28
0.4	12.78
0.5	13.26
0.6	13.80
0.7	14.42
0.8	15.06
0.9	15.61
1.0	16.00
1.1	16.52
1.19	16.85
1.31	17.3
1.35	17.5
1.55	18.4
1.71	19.1
1.77	19.4
1.83	19.82
1.85	20.12
1.89	20.48
1.91	20.96
1.93	21.24
1.93	21.40
1.93	21.70
1.99	22.26
2.03	22.86
2.09	23.32

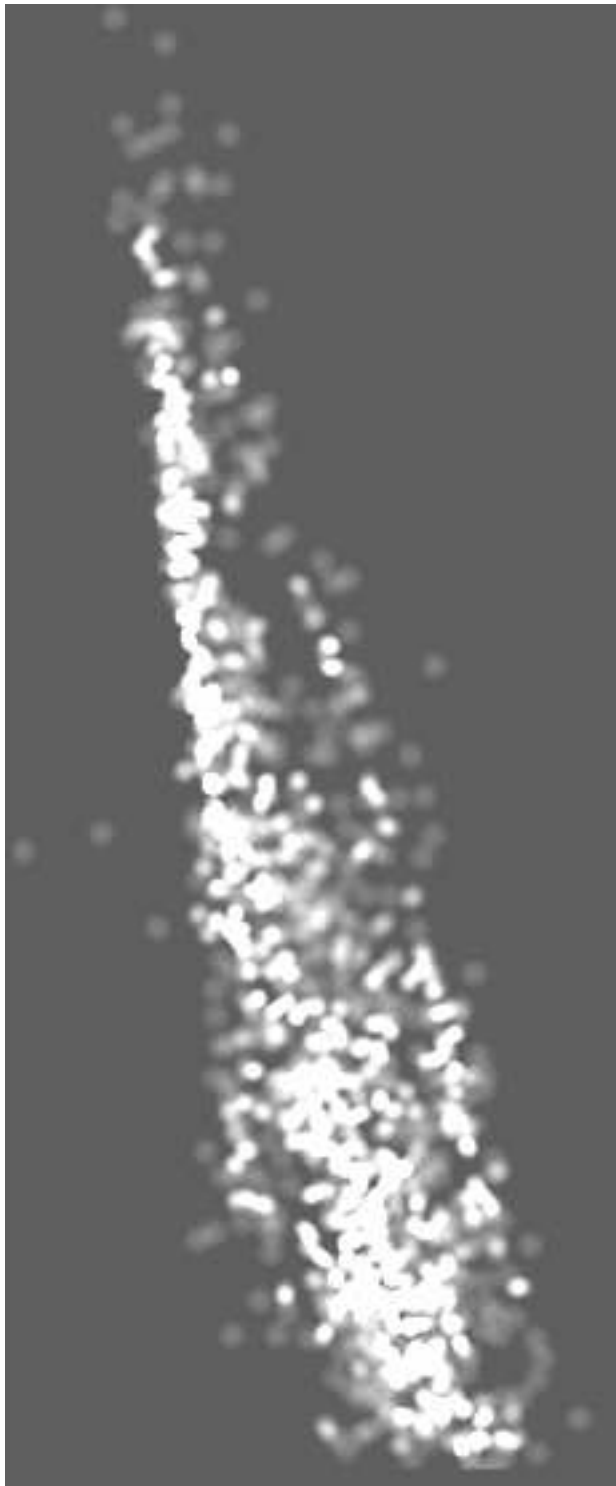
Table 3. *VI* Fiducial Main Sequence

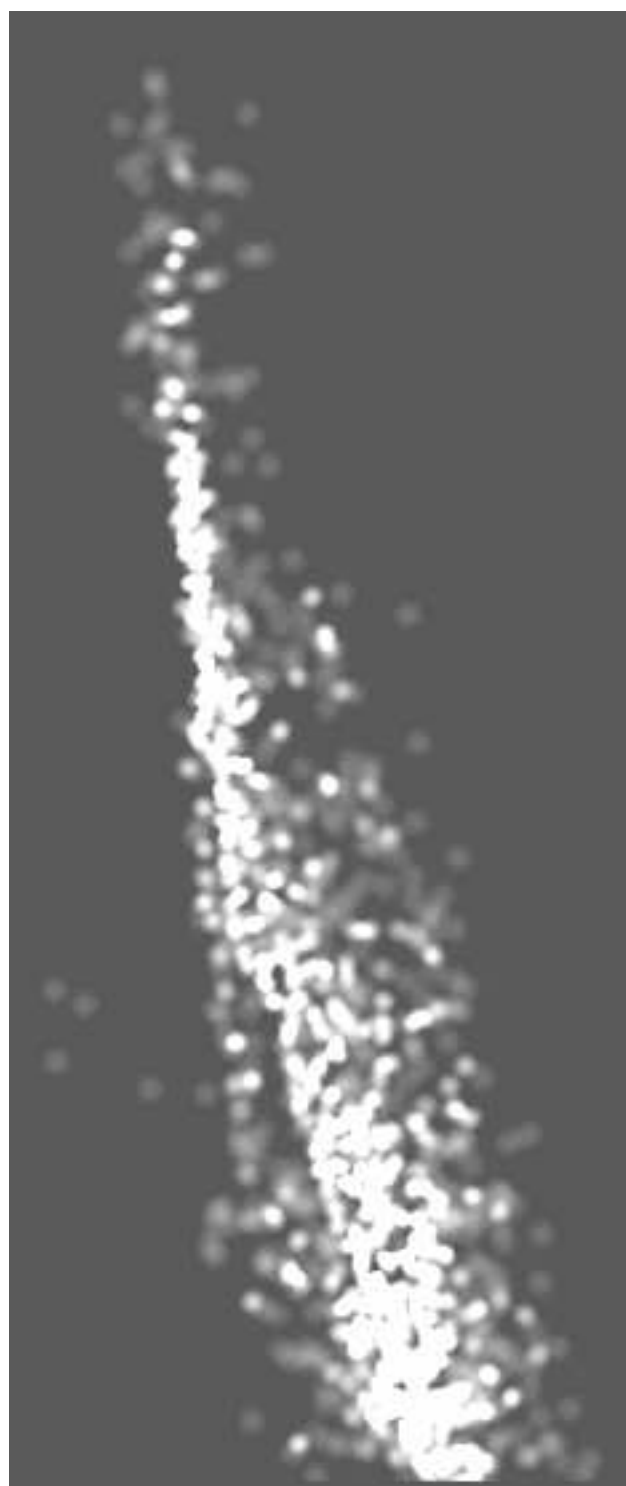
$V - I$	V
(1)	(2)
0.3	11.7
0.4	12.3
0.5	12.8
0.6	13.05
0.7	13.4
0.8	14.05
0.9	14.7
1.0	15.35
1.1	15.95
1.2	16.4
1.3	16.9
1.4	17.25
1.5	17.5
1.53	17.7
1.82	18.5
2.16	19.4
2.42	19.95
2.59	20.5
2.75	20.96
2.99	21.70
3.11	22.26
3.27	22.84
3.39	23.46
3.55	24.02
3.67	24.34
3.83	24.62

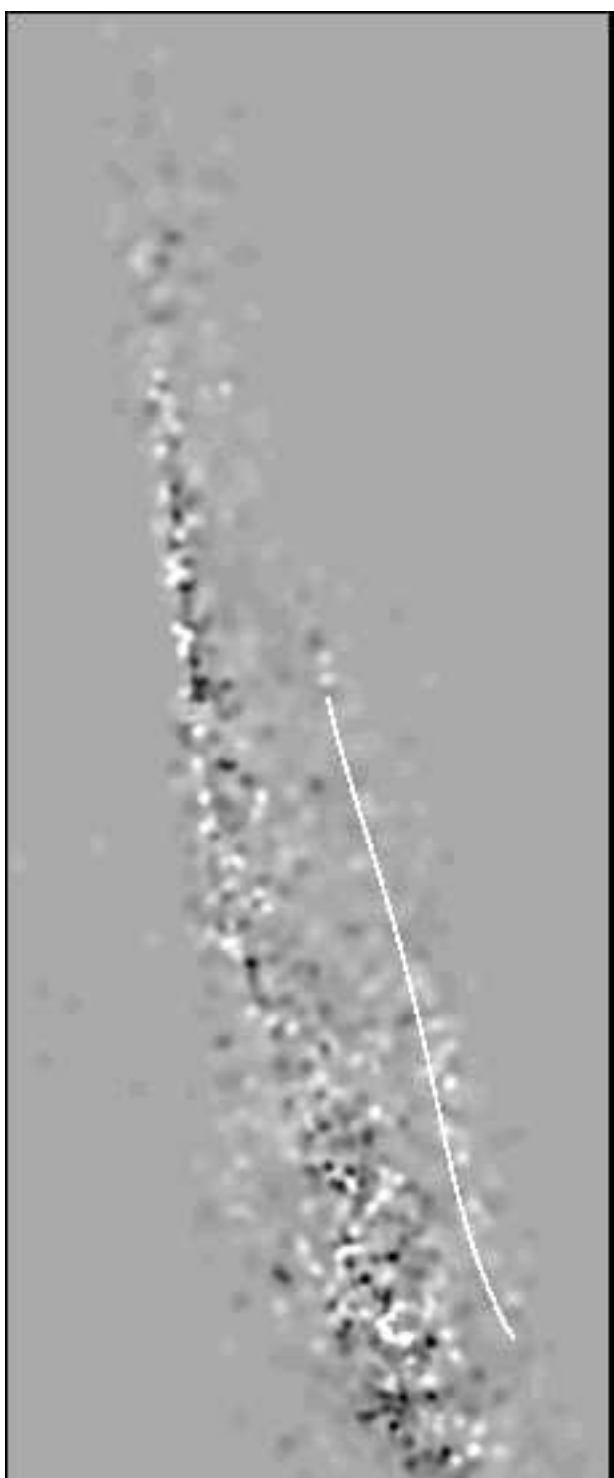


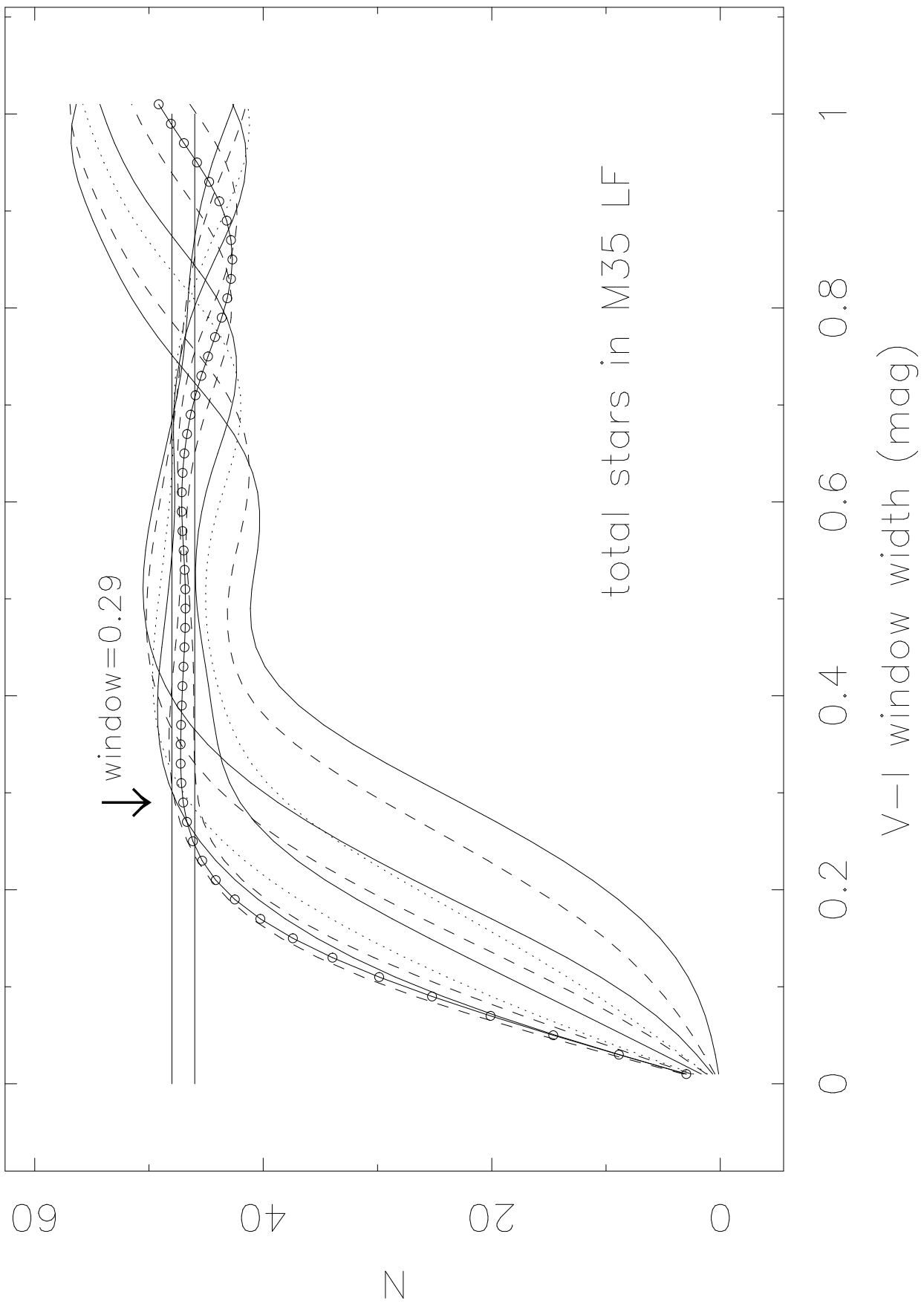


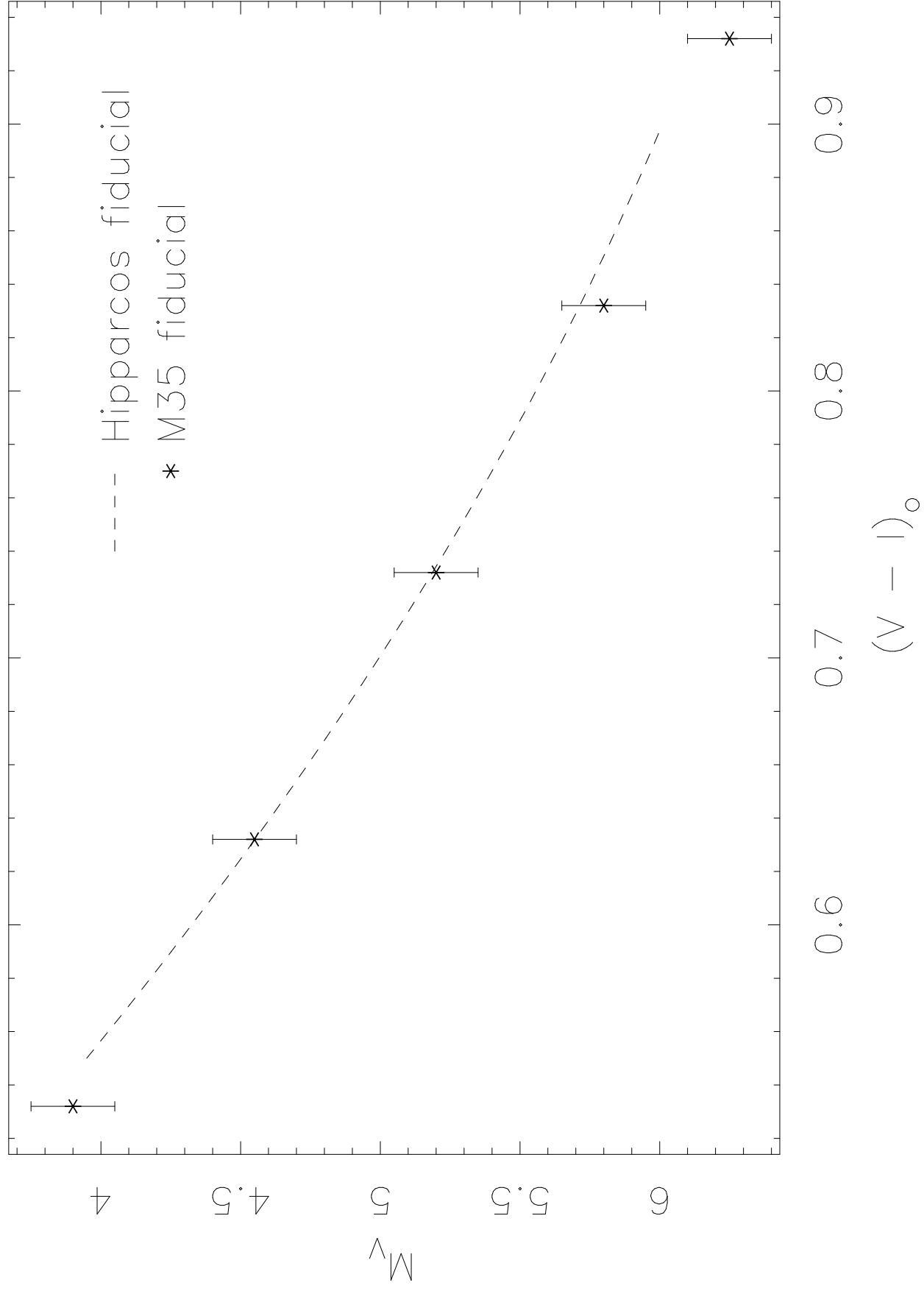


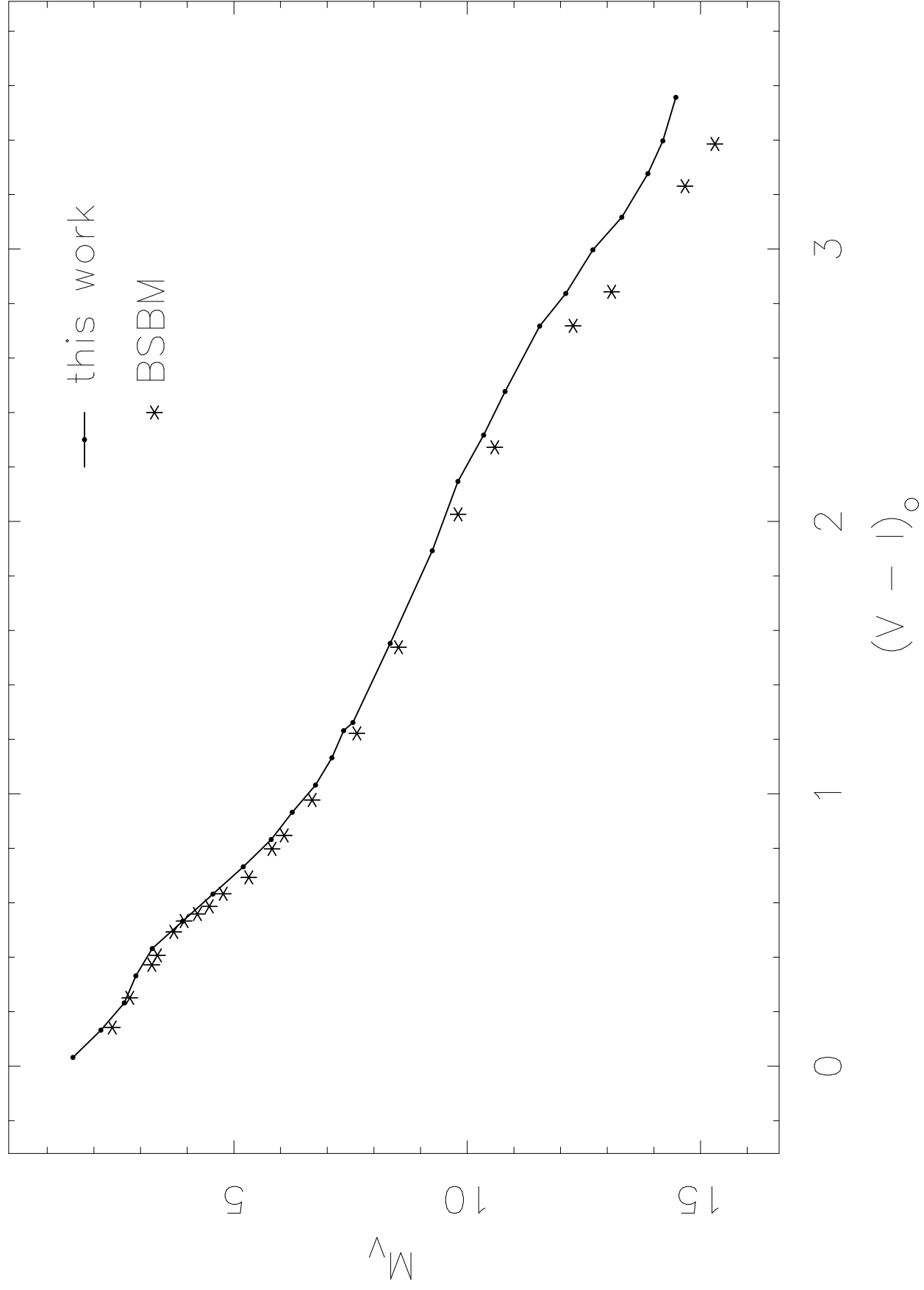


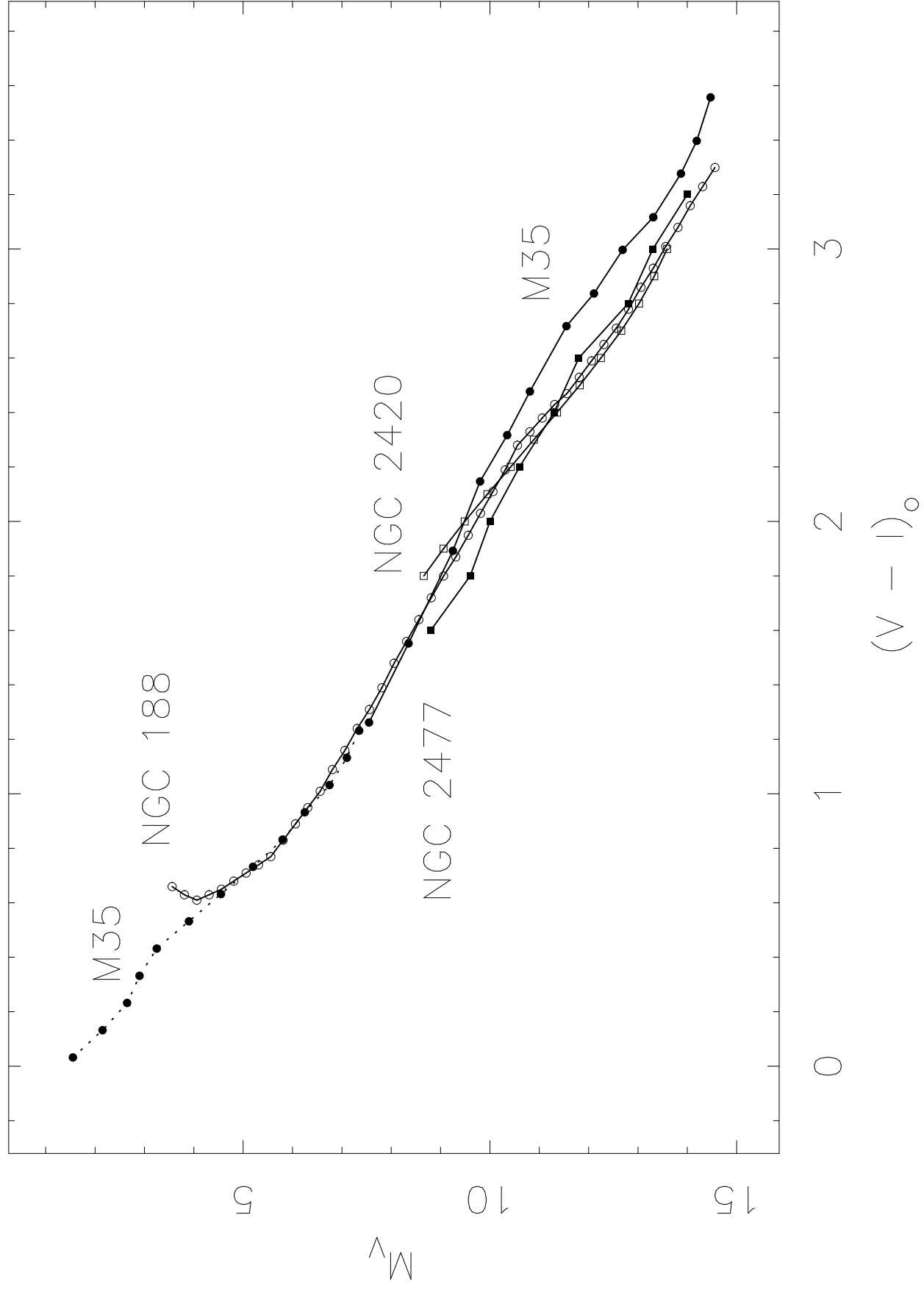


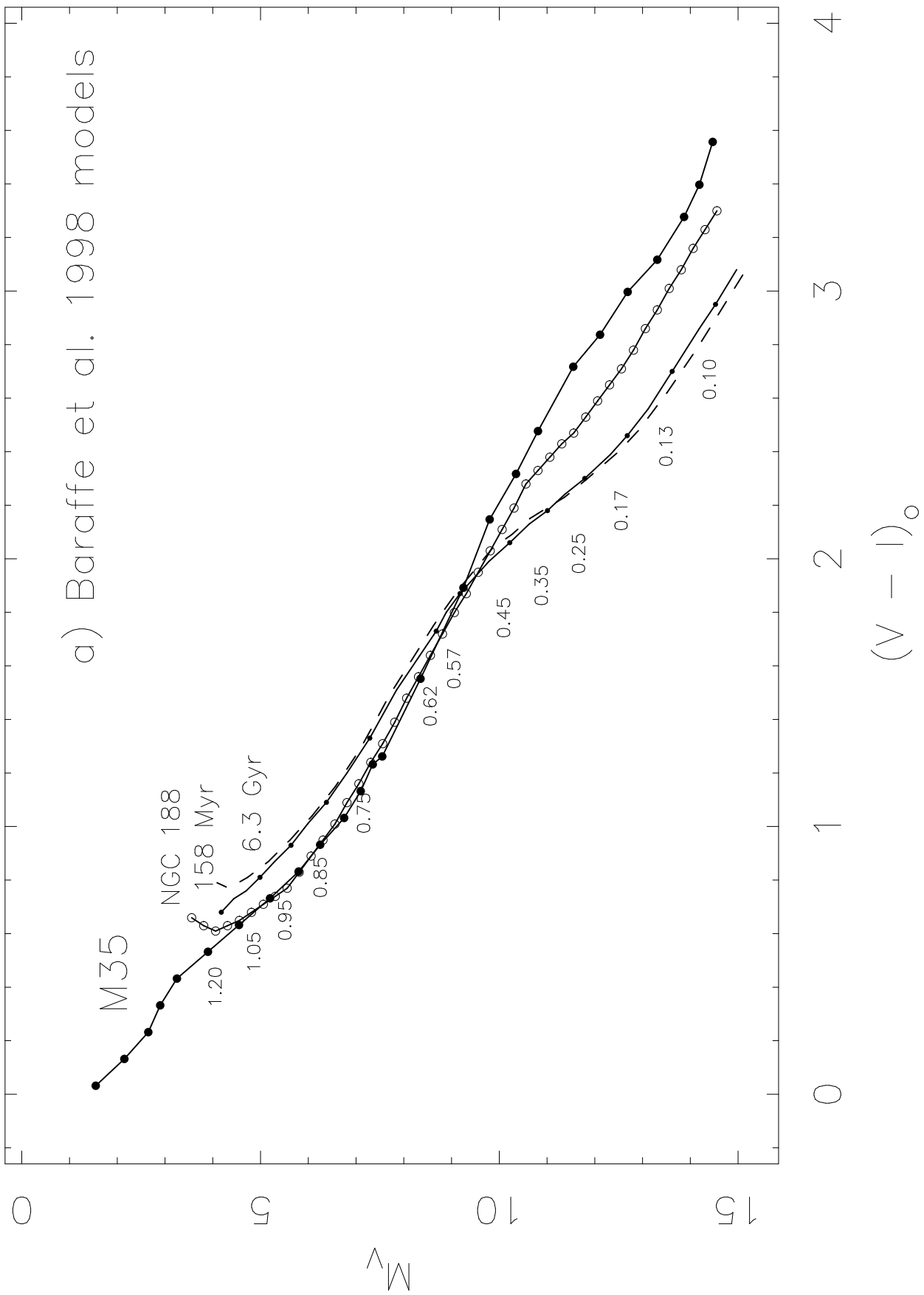


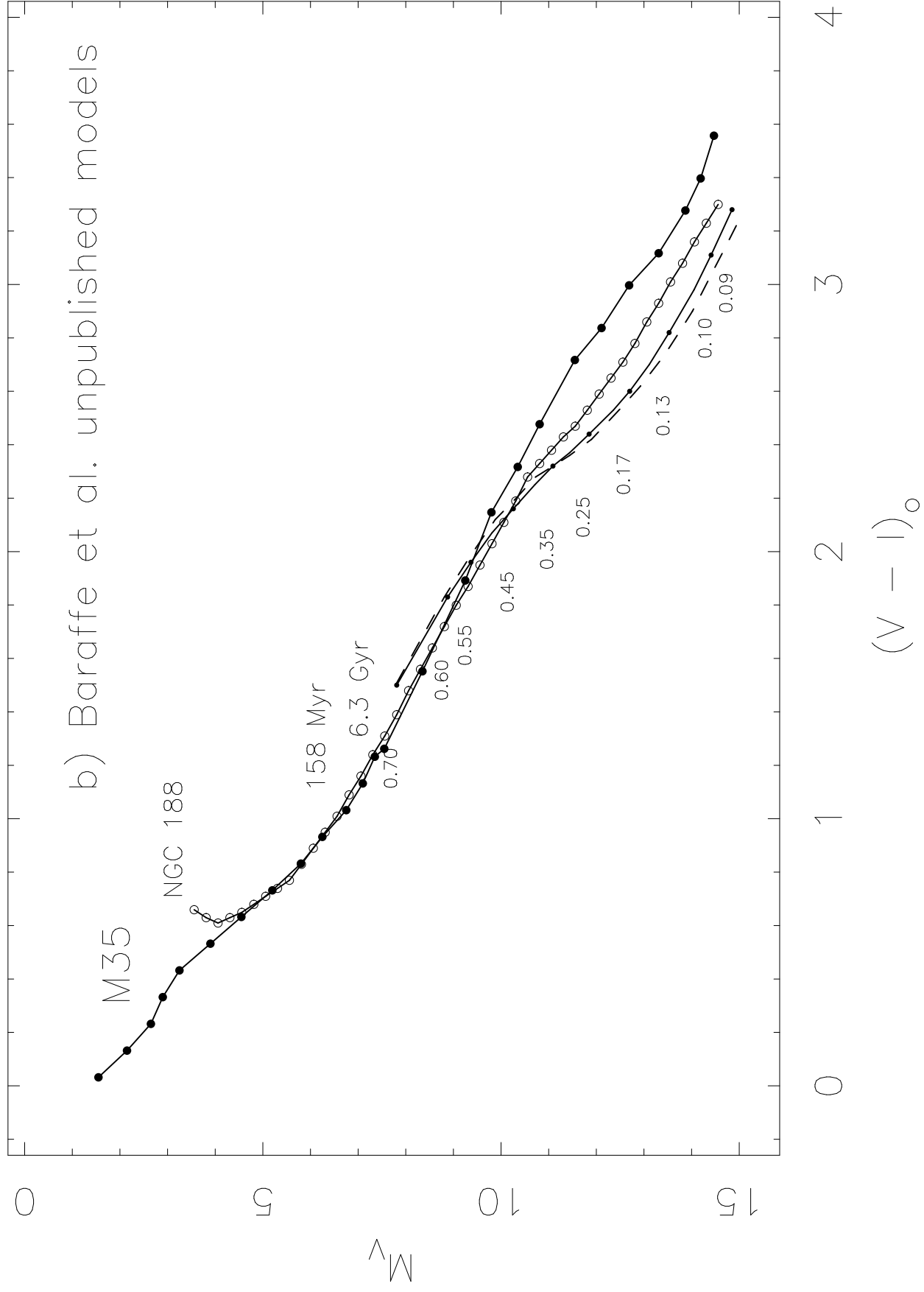


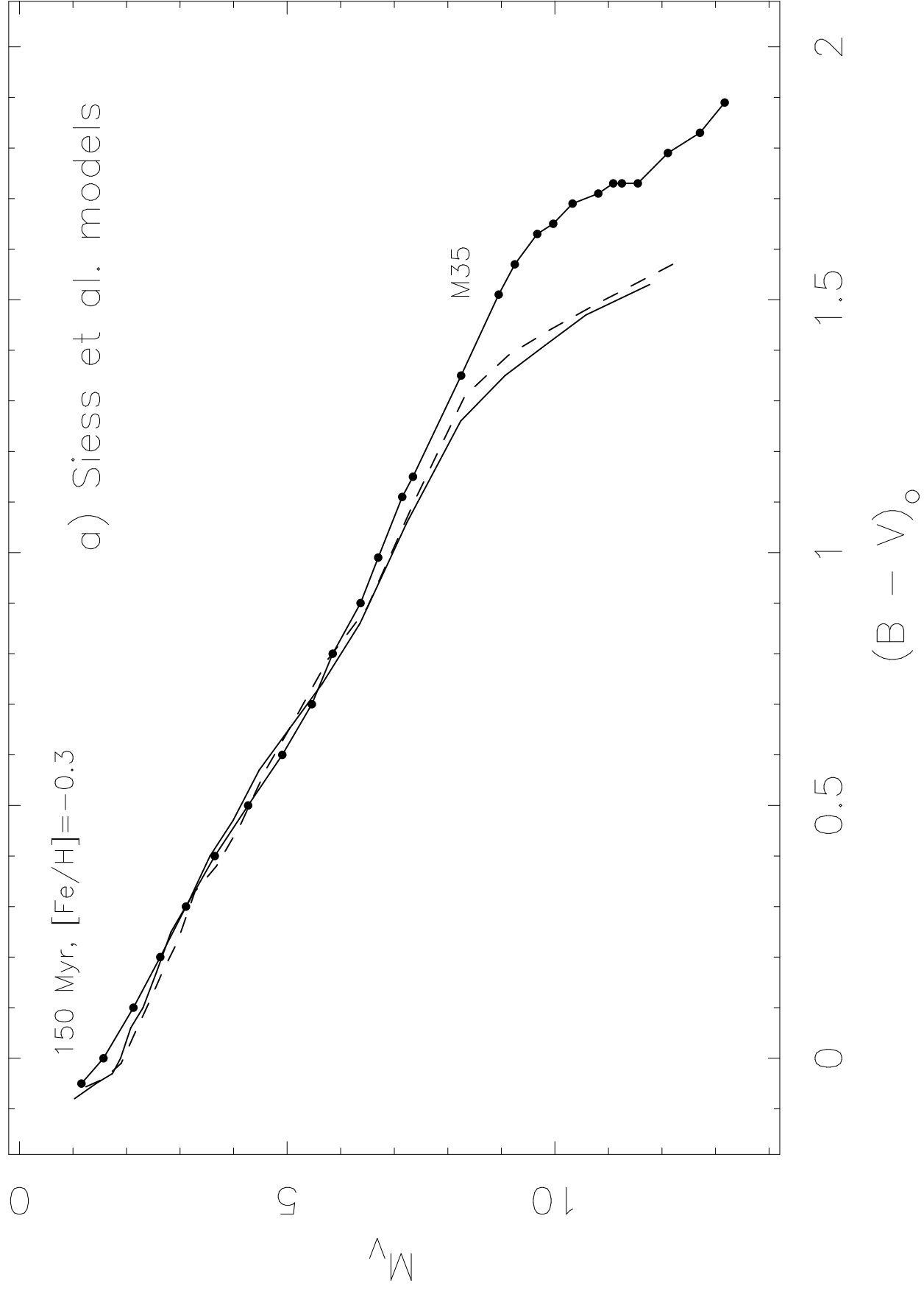


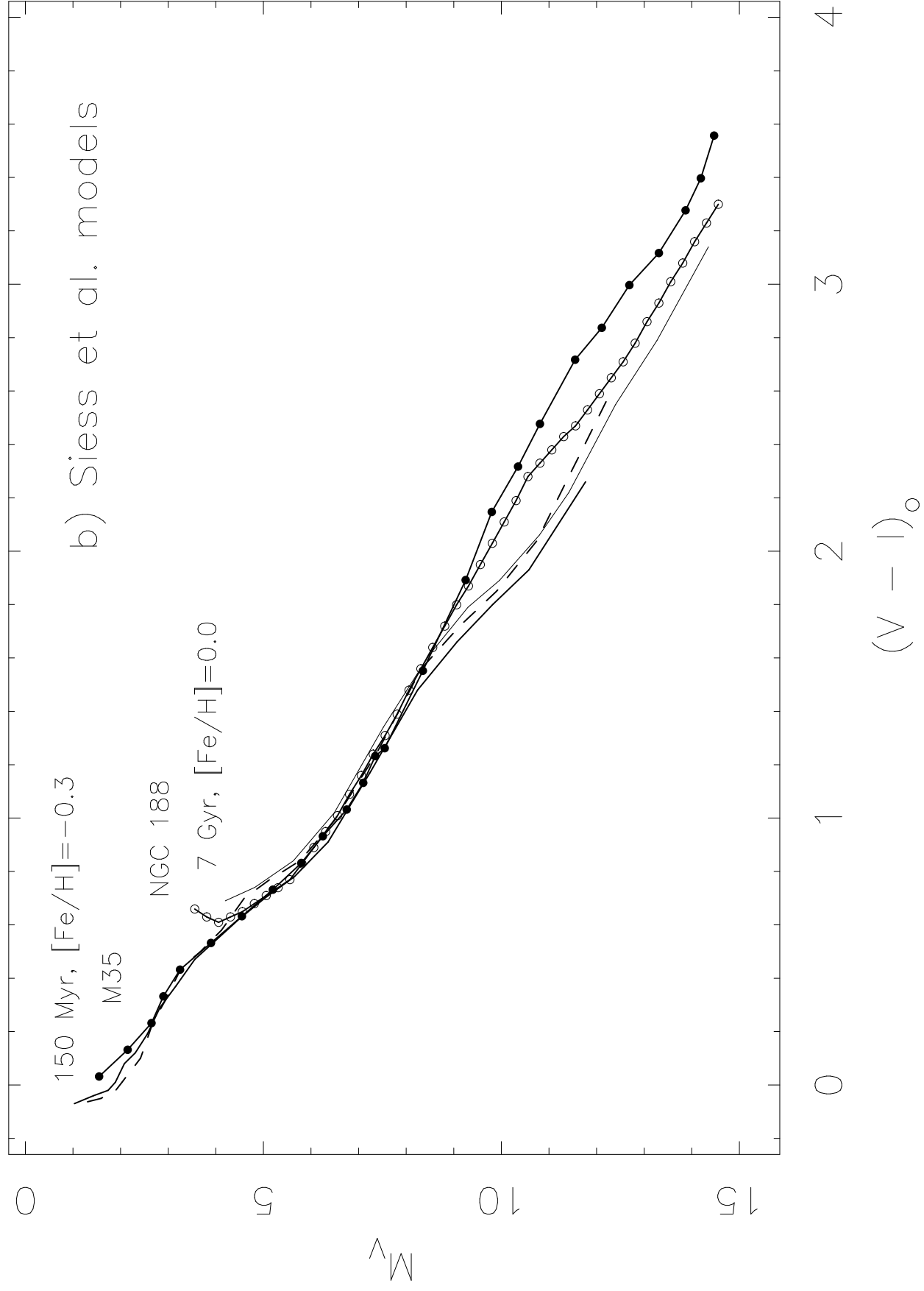


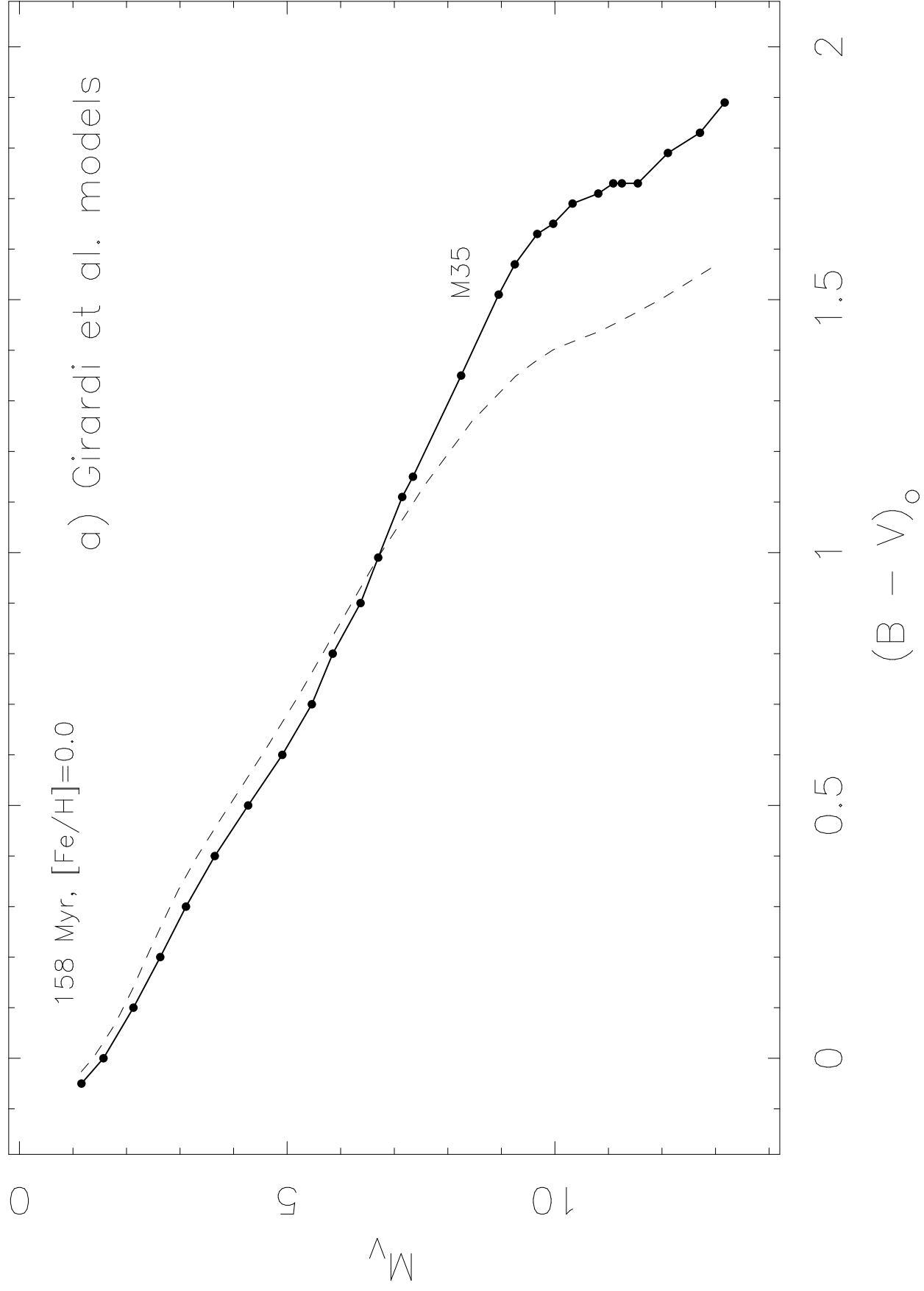


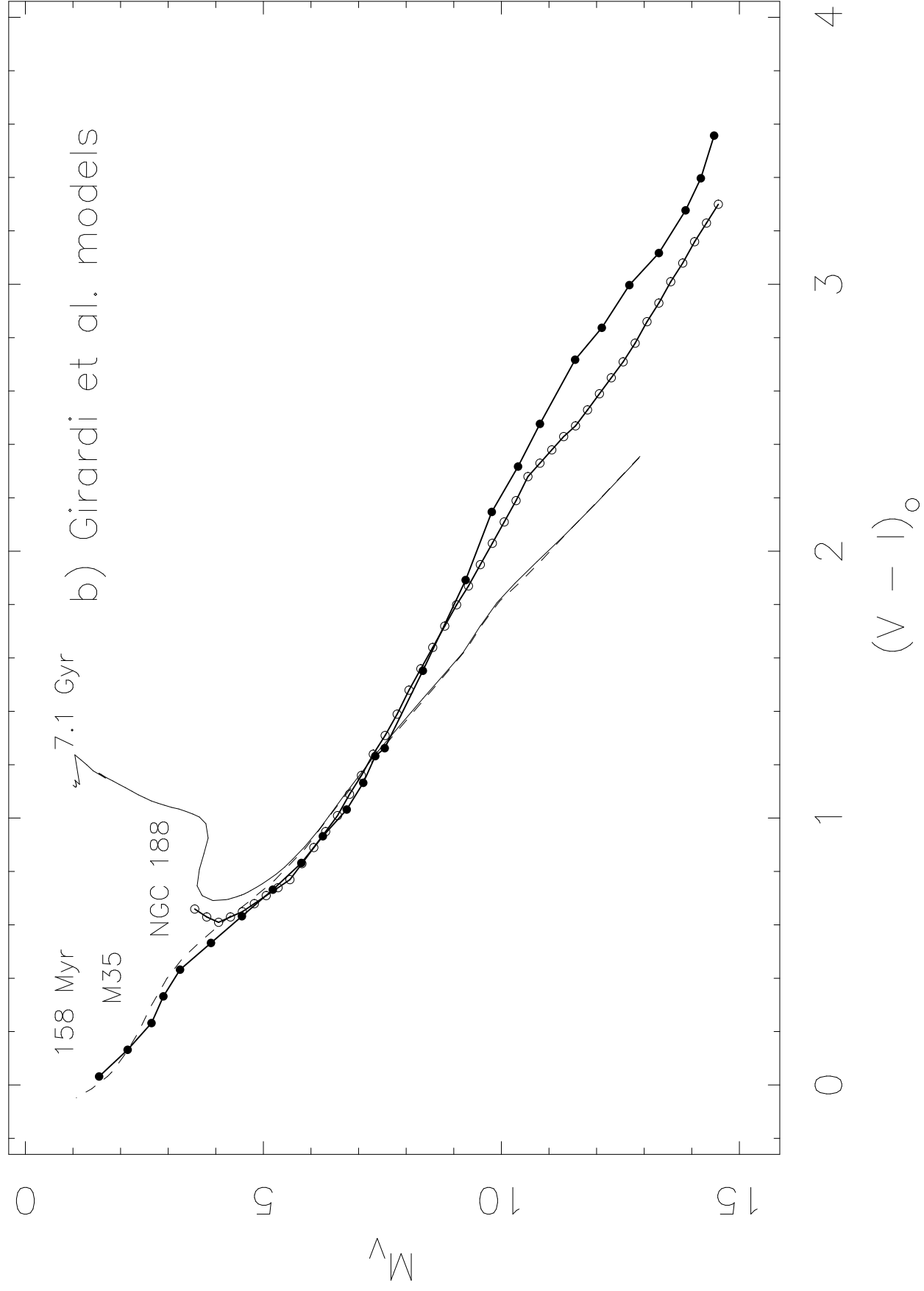


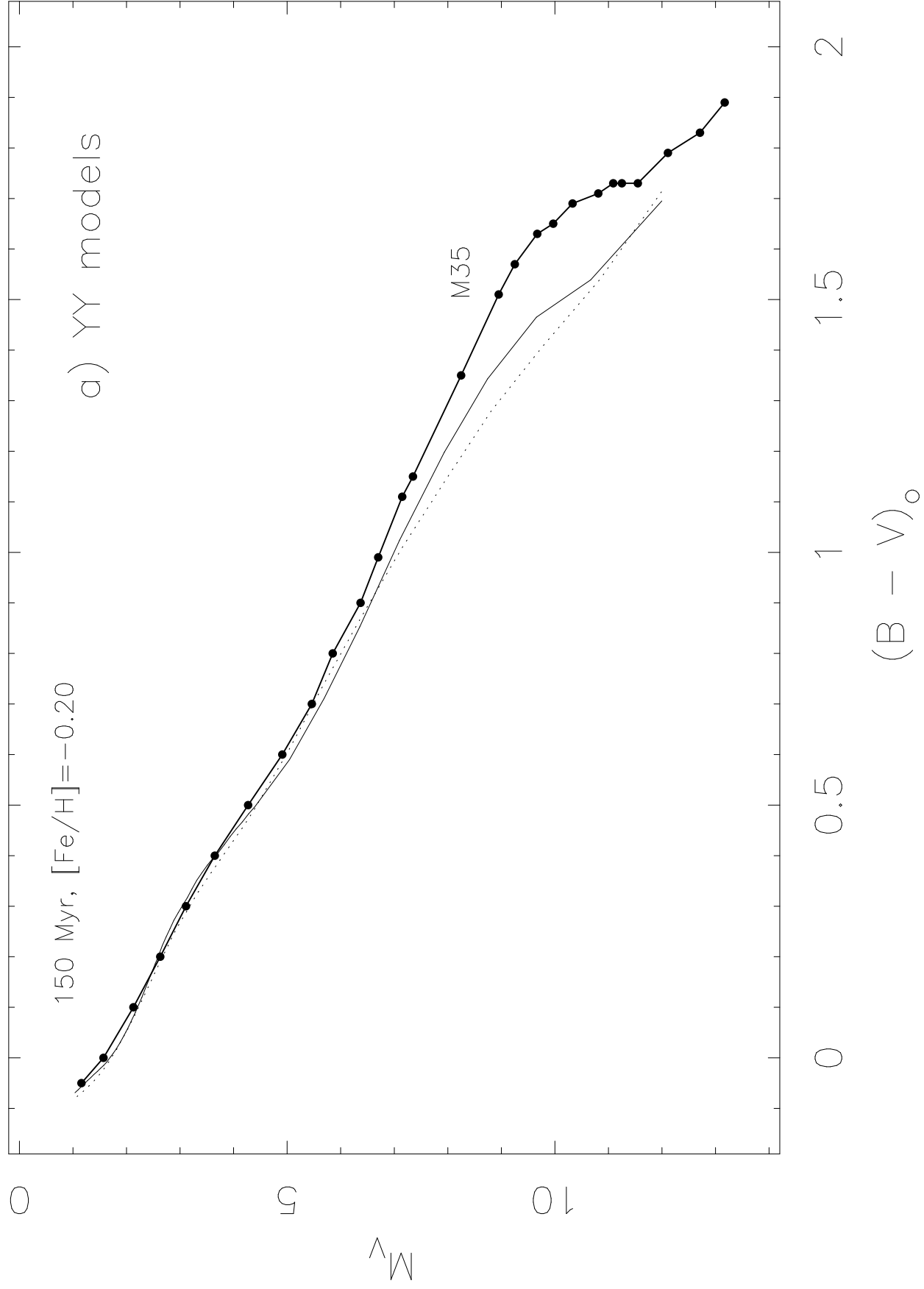


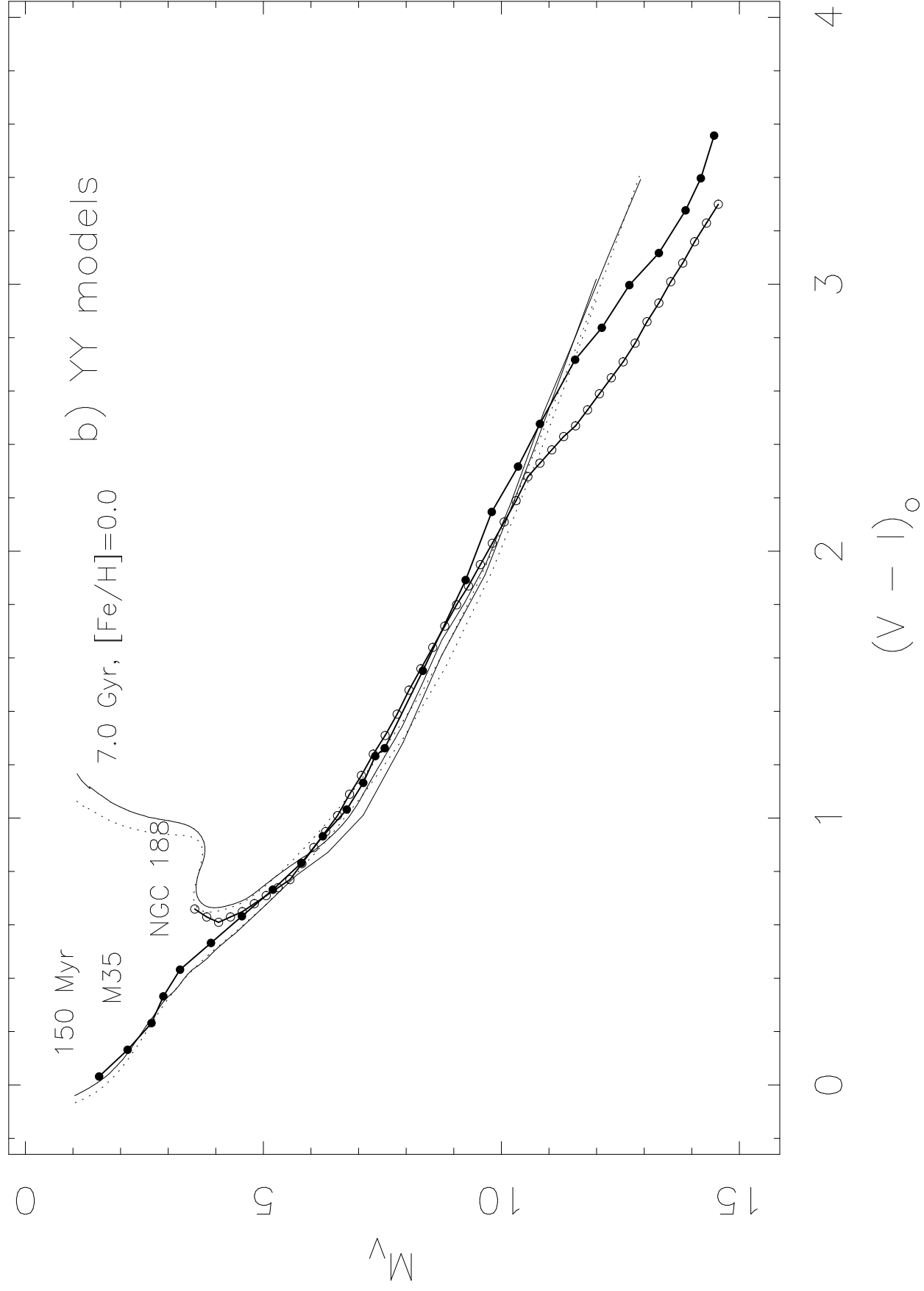


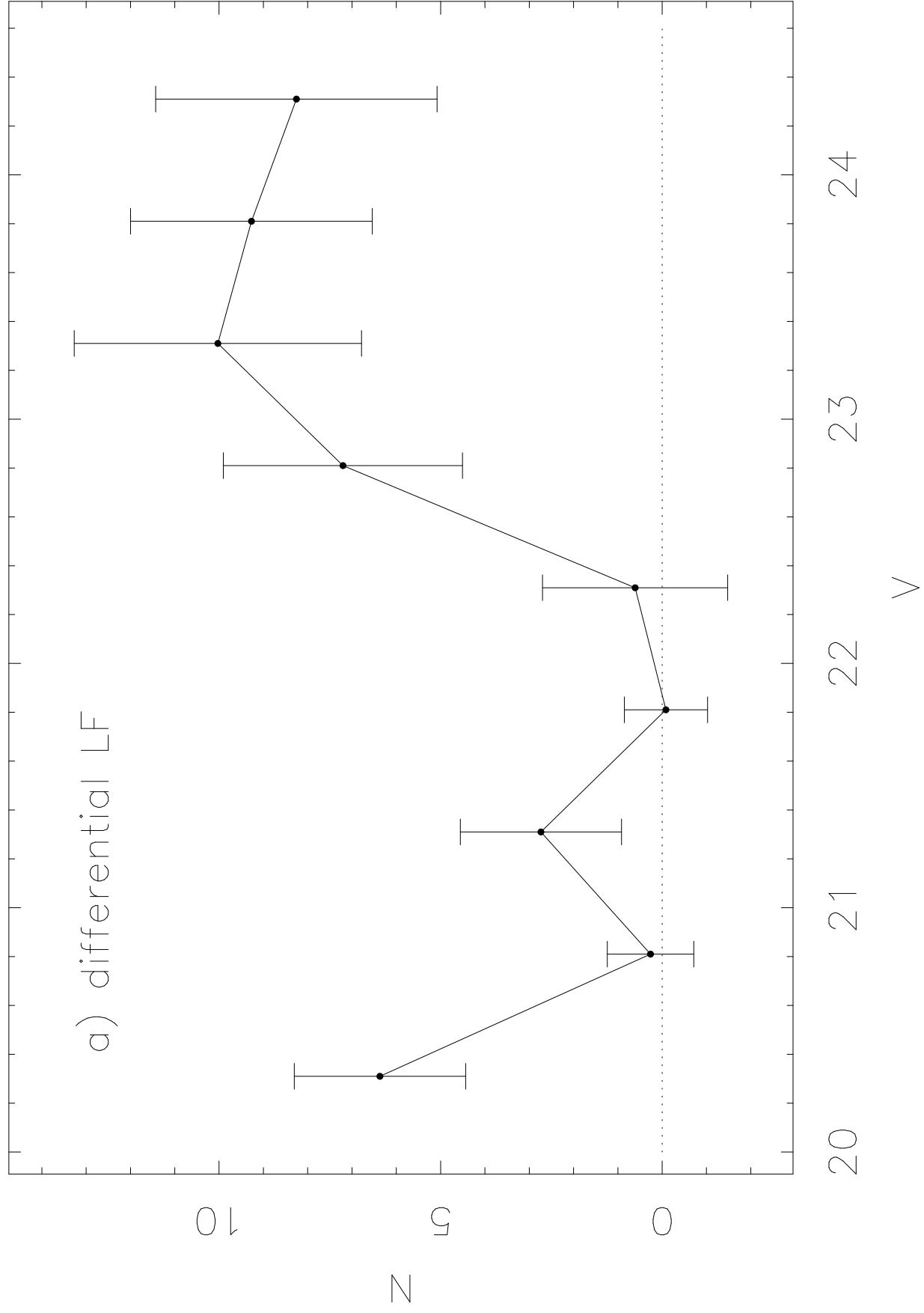


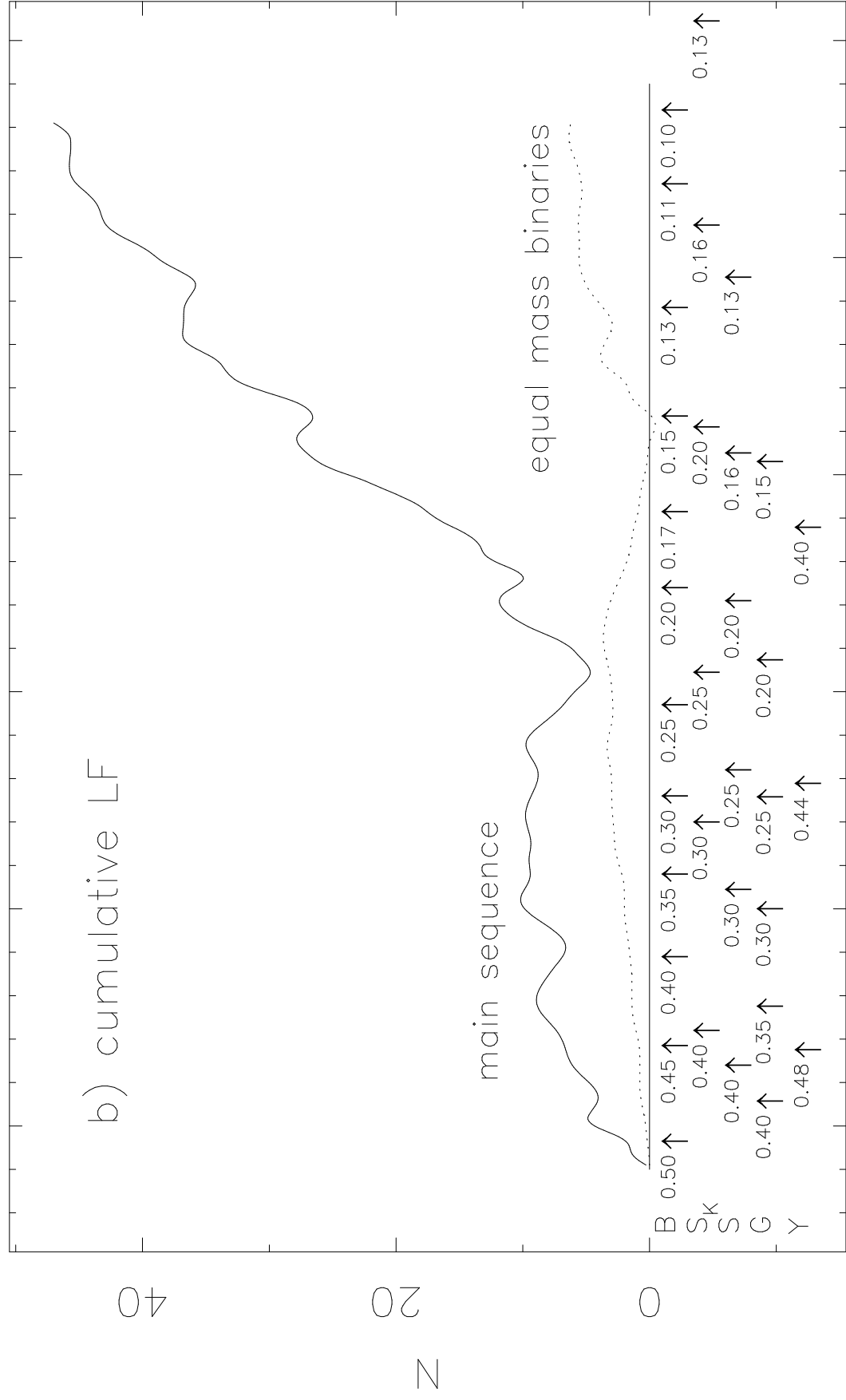












20 21 22 23 24 25

V

